



**Master Thesis carried out to obtain the following degrees:**

**Master Degree in Smart Cities and Communities (SMACCS)**

**&**

**Master Degree in Research in Energy Efficiency and Sustainability in Industry, Transportation, Building and Urban Planning (EESITBUP)**

Title:

Student:

Supervisor:

Academic Course:

Date:





# Dynamic and Transient Analysis of LVRT Augmented Grid Tied DFIG based Wind Turbine

**Student Name: Md Sajid Hossain**

Main academic Supervisor: Dr. Oihane Abarrategi, UPV/EHU.

**A Master Thesis submitted for the Erasmus Mundus Joint Master  
Degree on Smart Cities and Communities (SMACCS)**

June 2022

University of Mons, Heriot Watt University, International Hellenic University,  
University of the Basque Country





# Abstract

This thesis aims to present Low Voltage Ride Through (LVRT) augmentation of the grid-tied Doubly Fed Induction Generator (DFIG) based wind turbine. Voltage stability is a critical grid code criterion that must be strictly adhered. A substantial voltage drop happens during a fault or network disruption situation, which must be restored as quickly as possible. According to modern grid code standards, 90 percent of the voltage must be restored to pre-fault levels in 1500 milliseconds. As a result, both dynamic and transient assessments are performed to evaluate the intended power system's LVRT capabilities. In this study, fault analysis including the most severe 3LG fault under transient conditions has been examined in order to evaluate the tuned PI controller scheme and resilience of the developed power system model. PSCAD/EMTDC® v4.5 tool has been used extensively to develop the DFIG wind turbine aerodynamic model, DFIG control scheme and power system model analysis. Simulation results show that tuned Proportional Plus Integral (PI) controllers effectively augment the LVRT functionality by injecting sufficient reactive power into the grid during fault or network disturbance scenarios.

**Keywords:** LVRT, DFIG, PI Controller, Grid-Tied, Wind Turbine, Dynamic Analysis, Transient Analysis, Augmentation, Enhancement.

Md Sajid Hossain

June 19, 2022



# Table of Contents

<b>ABSTRACT.....</b>	<b>III</b>
<b>TABLE OF CONTENTS.....</b>	<b>V</b>
<b>1 INTRODUCTION.....</b>	<b>1</b>
1.1 CONTEXT AND MOTIVATION .....	1
1.2 CHALLENGES.....	1
1.3 OBJECTIVES .....	2
1.4 ELEMENTS OF METHODOLOGY .....	2
1.5 PLANNING OF THE CHAPTERS .....	3
<b>2 LITERATURE REVIEW .....</b>	<b>5</b>
2.1 CARBON EMISSION AND RENEWABLE ENERGY.....	5
2.2 WIND ENERGY SCENARIO.....	7
2.3 WIND ENERGY INTEGRATION: ISSUES AND CHALLENGES.....	8
2.4 VOLTAGE STABILITY .....	8
2.5 LVRT GRID CODE REQUIREMENT FOR WIND POWER .....	9
2.6 STRATEGIES TO AUGMENT LVRT OF WIND FARM.....	10
2.7 GRID CODE CRITERIA OF FREQUENCY OPERATING RANGE .....	12
2.8 HYBRIDIZATION OF WIND TURBINE SYSTEM .....	13
2.9 CHAPTER SUMMARY .....	15
<b>3 MODELLING OF WIND TURBINE .....</b>	<b>17</b>
3.1 TOPOLOGY OF WIND ENERGY TECHNOLOGY.....	17
3.2 WIND TURBINE SYSTEM COMPONENTS.....	18
3.3 EXTRACTED OUTPUT POWER OF THE WIND TURBINE .....	20
3.4 MODELLING DRIVE TRAIN SYSTEM.....	22
3.5 CONTROLLER FOR PITCH ANGLE.....	23
3.6 INDUCTION MACHINE CHARACTERISTICS .....	24
3.7 WRIG MODEL.....	24
3.8 VSWT-DFIG BASED CONFIGURATION.....	25

3.9	CHAPTER SUMMARY.....	26
<b>4</b>	<b>DFIG CONTROL SCHEME .....</b>	<b>27</b>
4.1	TWO LEVEL POWER CONVERTER .....	27
4.2	DC LINK CIRCUIT.....	28
4.3	DETAILED CONFIGURATION OF DFIG .....	28
4.4	PI CONTROLLER .....	29
4.5	ROTOR SIDE CONTROLLER .....	30
4.6	GRID SIDE CONTROLLER .....	32
4.7	CHAPTER SUMMARY.....	33
<b>5</b>	<b>RESULTS AND ANALYSIS .....</b>	<b>35</b>
5.1	POWER SYSTEM MODEL .....	35
5.2	DYNAMIC STABILITY PERFORMANCE ANALYSIS.....	36
5.3	TRANSIENT STABILITY PERFORMANCE ANALYSIS .....	42
5.4	CHAPTER SUMMARY.....	49
<b>6</b>	<b>CONCLUSION AND FUTURE WORK .....</b>	<b>51</b>
	<b>BIBLIOGRAPHY .....</b>	<b>55</b>

# 1 Introduction

Over the past several years, renewable energy resources have been on key focus for the ever-growing need for power and major environmental impacts due to the use of fossil fuels. The world is already facing a “climate emergency” situation from “climate change”. In many areas, renewable energy sources (RESs) have emerged as promising energy sources due to significant technological developments, falling resource prices and higher levels of competitiveness.

## 1.1 Context and Motivation

Renewable energy resources play a critical role in our day to day life due to the nature of abundant availability, no fuel cost, lower or almost no environmental impact, reliability of electricity supply in decentralized applications, etc. Among numerous Renewable Energy Sources (RESs) such as solar, wind, tidal, geothermal, bioenergy, hydro, etc. wind and solar power are becoming very popular and technology is developing very fast. Both solar and wind power have their pros and cons; determining which technology is superior is very dependent not only on the application, but also on the location of the system. However, a wind turbine can produce electricity around the clock as long as there is wind, but solar panels can only do so when exposed to sunlight. Therefore, the ever-growing demand for wind or solar energy in the existing power grid impacts the power system's transient and dynamic stability. During a fault or a network disturbance situation, the voltage and frequency stability of the power system is an important concern. For the consistency and dependability of the operation of renewable energy sources, additional researches need to be carried out. In this thesis work, the voltage stability issue has been analysed by maintaining grid code criteria under different fault or network disturbance situations.

## 1.2 Challenges

Generating energy from intermittent renewable resources and supply to the grid requires to follow strict compliance regulations. A grid code sets standards, especially voltage and



frequency regulations for Transmission System Operators (TSO) and enforces them to maintain strictly. Earlier, renewable energy generations were not significant thus grid code was not enforced in RES. Due to the large penetration of RES, the modern grid code enforces strict guidelines for the large-scale integration of RES into the power grid. Most importantly grid code sets standards for the stability of the power grid system. Hence, maintaining grid code standards for RES integration into the power grid is a challenging task.

Large-scale wind turbine integration into the electrical grid poses a substantial challenge in terms of system stability. When it comes to system stability, a wind turbine must meet grid code standards depending on the network situation. One of the most important grid code criteria for analysis is Low Voltage Ride Through (LVRT). In order to comply with the modern grid code standards, 90 percent of the voltage must be restored to pre-fault levels in 1500 milliseconds or 1.5 seconds after the fault. Moreover, in the event of grid failures or other network disturbances, wind turbines are needed to inject the maximum required reactive power into the grid to maintain the grid voltage stable. So, the challenge lies here in how quickly the grid voltage recovers to the rated condition by injecting the maximum amount of reactive power.

### **1.3 Objectives**

This thesis work emphasizes the following key objectives:

- To develop a model of wind turbine based on Doubly-Fed Induction Generator (DFIG).
- To derive all the required aerodynamic mathematical modelling of DFIG
- To tune the PI controller's proportional and integral parameter constant to augment LVRT functionality.
- Utilising the PSCAD/EMTDC simulation tool to analyse both dynamic and transient voltage stability performance of the tuned controller.

### **1.4 Elements of Methodology**

The following key methodologies have been applied to design and analyse different situations concerning the scope of the work.

- Design of the detailed Wind Turbine Model
  - Modelling of the Drive Train System
  - The controller for pitch angle
- Design of the Power System
  - Assessment of various fault scenarios
  - Control Scheme to augment LVRT functionality
  - Voltage stability analysis focusing on grid code requirements

## 1.5 Planning of The Chapters

In chapter 2, a comprehensive literature assessment has been conducted to identify current research trends in the area of wind energy's grid integration. Furthermore, recent statistical data has been provided to assess the future of wind energy and its contribution to overall energy production. Other fossil fuels and renewable energy sources are also included in this chapter to better understand the effect of CO<sub>2</sub> emissions.

Chapter 3 aims to present a system model of the wind turbine and various characteristics curves related to the turbine. Different types of wind energy conversion topologies are discussed. Later, an overview of wind turbine components, details of extracted power, drive train model and pitch controller concepts have been illustrated for varying speed turbine systems. Finally, the detailed model of the DFIG wind turbine has been presented.

Chapter 4 illustrates DFIG control schemes including rotor and grid side controllers. To achieve stability during fault or network disturbance situations, PI controllers with optimized proportional and integral constant parameters have been used in RSC and GSC. A two-level semiconductor power converter including a DC link circuit and protection control scheme has also been addressed.

In chapter 5, simulation results are presented and comprehensive analysis has been performed to realize the robustness of the designed model. A power system model has been considered for the assessment of different faults or network disturbance situations. For that PSCAD/EMTDC simulation tool has been used extensively to model the power system and analyse the effectiveness of the tuned PI controllers.

Finally, in Chapter 6, the general findings of all the chapters about this work are stated. The future scope related to this work has also been presented in this chapter.

## 2 Literature Review

This chapter aims to present a comprehensive literature review to identify the trending research area in the field of integrating wind energy into the grid. Besides, statistical data from recent years have also been presented to perceive the future of wind energy and its contribution to total energy generation. Environmental impacts considering other fossil fuels and renewable sources are also addressed in this work to understand the impact of CO<sub>2</sub> emissions.

### 2.1 Carbon Emission and Renewable Energy

High dependency on fossil fuels is creating ecological contamination and safety hazards, which are increasingly becoming a major concern in society. The term "climate change" has already been replaced with "climate emergency". According to the recent Global Energy Review of the International Energy Agency (IEA), all fossil fuels are expected to see considerable increases in demand over the years. Coal consumption is predicted to rise more than demand for all renewable sources combined, resulting in a roughly 5% increase in emissions [1]. Table 2.1 shows emissions of CO<sub>2</sub> per MWh of electricity generation from various sources.

Table 2.1: CO<sub>2</sub> emissions per MWh of electricity generation from different sources [2]

Sources	CO <sub>2</sub> emissions in Kg (per MWh)
Coal	1000
Natural Gas	430
PV	60 – 100
Wind	3 - 22
Hydro	4

Whilst a lot of emphasis is set on the reduction of CO<sub>2</sub>, it is imperative to divert attention to the technologies of carbon capture, storage and reuse too. Besides, a worldwide 'carbon tax' would be logical and might be an effective strategy to ensure global fairness by minimizing the terrible impacts of global warming. Thus, businesses and individuals will take

necessary initiatives to lessen their emissions such as adopting new technologies or switching fuels and focusing on renewable energy sources. Accelerated renewable energy deployment and improved energy efficiency may accomplish over 90% of the energy-related CO<sub>2</sub> emissions reductions required by 2050 to put the world on an energy path to fulfilling the Paris climate commitments [3].

In the context of decarbonization, renewable energy research has been a pressing issue in recent years because of the continual depletion of fossil fuels and the ever-increasing electricity demand. Due to significant technology breakthroughs and declining resource costs as well as increased competitiveness, in many regions, RES has become one of the most favourable energy resources [4]. Although the RES has a higher initial capital investment, in the long run, RES provides good prospects in terms of sustainability and energy cost. Green energy is important in the energy transition because it has a minimal environmental effect and might even be used as a substitute for non-renewable energy [5]. Green or renewable energy penetration has increased significantly over the previous decade, where several nations now producing more than half of their energy requirements from renewable sources and aiming toward 100% renewables. [6]–[9]. Attractive potential and compelling requirements are accelerating the world's energy system to a new level of transformation (as shown in figure 2.1).

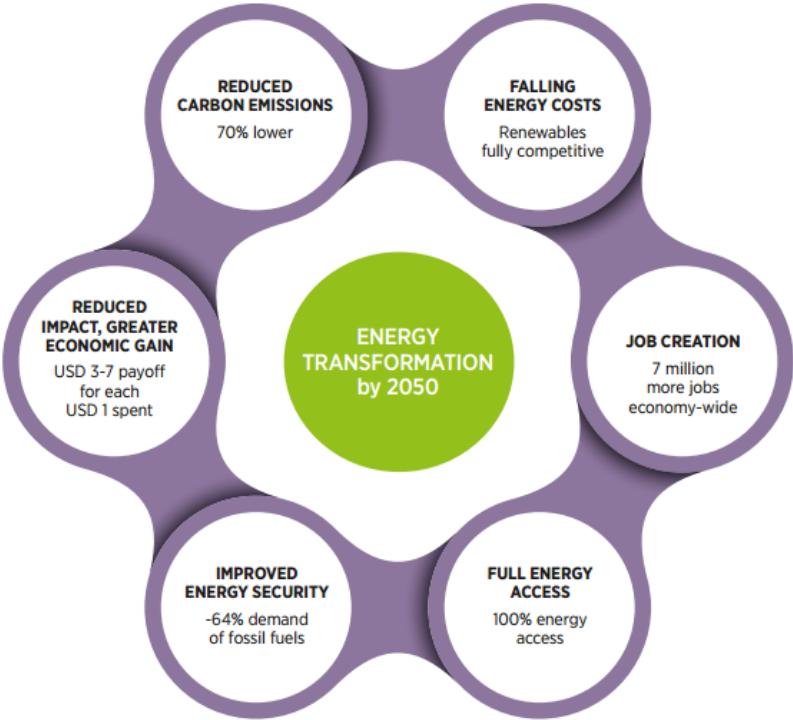


Figure 2.1: Transformation of the world's energy system [3].

## 2.2 Wind Energy Scenario

While there are many various types of renewable energy resources, including solar photovoltaic, wind, biomass, biogas, tidal and geothermal, etc., wind energy and solar photovoltaic (PV) systems play a substantial role in the global energy market and compete with the conventional electricity industries. Large-scale wind turbines and solar photovoltaic systems are expected to provide supplementary services to the grid in addition to supplying grid power. According to the Renewable 2021 Global Status Report [10], the total installed capacity of RESs in 2019-2020 is given in figure 2.2.








POWER		2019	2020
Renewable power capacity (including hydropower)	GW	2,581	<b>2,838</b>
Renewable power capacity (not including hydropower)	GW	1,430	<b>1,668</b>
 Hydropower capacity <sup>2</sup>	GW	1,150	<b>1,170</b>
 Solar PV capacity <sup>3</sup>	GW	621	<b>760</b>
 Wind power capacity	GW	650	<b>743</b>
 Bio-power capacity	GW	137	<b>145</b>
 Geothermal power capacity	GW	14.0	<b>14.1</b>
 Concentrating solar thermal power (CSP) capacity	GW	6.1	<b>6.2</b>
 Ocean power capacity	GW	0.5	<b>0.5</b>

Figure 2.2: Total installed capacity of RESs in 2019-2020 [10].

Wind energy is demonstrating its effectiveness as a viable solution for meeting energy demand that is generated without the use of fossil fuels, the emission of greenhouse gases (GHG) and freshwater for cooling and/or harmful air pollutants by making a tangible contribution to clean and secure power production [11]. Wind energy has attracted a lot of interest from researchers because of its high efficiency, maximum power point monitoring capabilities, better power quality and self-control regulation of active and reactive power [12]–[15].

According to the forecast of the International Renewable Energy Agency (IRENA), by 2050, wind energy would produce more than one-third of total world power demands, making it the dominant generating source [3]. Figure 2.3 demonstrates yearly increases in global wind power capacity, 2010-2020 [10].

Based on a working report by Global Wind Energy Council (GWEC), wind power might reach 2110 GW by 2030, enough to generate up to 20% of global energy [16].

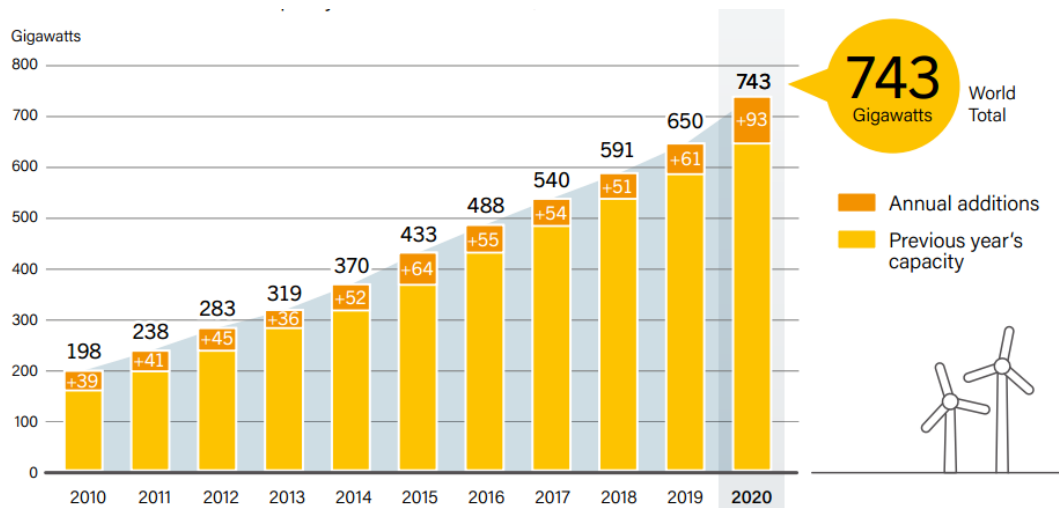


Figure 2.3: Yearly increases in global wind power capacity, 2010-2020 [10].

## 2.3 Wind Energy Integration: Issues and Challenges

Integration of renewable energy resources, particularly large-scale wind power considering the existing power system is a complicated issue for power system engineers. Due to the intermittency of renewables, power generated by wind is not stable. Power demand always needs to be matched by supply. Besides, power fed into the grid by generators needs to match the grid frequency and phase. Mostly, the wind turbines are far away from points of connection to the grid and cause grid integration issues mainly the harmonics disturbance along with variable output that would cause voltage fluctuations [17], [18]. As interface devices, various kinds of power electronic converters are now in use to maximize energy production from renewable energy systems. Such technologies are becoming more complicated as the need for renewable energy grows. Power system stability becomes a burden for transmission and distribution operators. As a result, extra control mechanisms for the wind turbine/solar PV combination are required and further research is required to attain a higher degree of RES penetration in the grid system.

## 2.4 Voltage Stability

Voltage stability implies to the capability of an electrical power system to sustain proper voltages on all associated buses during normal operation as well as after being exposed to a fault or network disruption. The system reaches to a state of voltage instability due to an uncontrolled voltage dip when a fault or network disturbance situation occurs in the power system. The fundamental source of voltage instability is the failure to meet the demand for reactive power [18].

Voltage stability and control issues are not new to the electrical utility sector, but they are getting a lot of attention nowadays, due to the ever-growing integration of renewable energy resources into the power grid. Voltage instability, which was traditionally linked only with weak systems and lengthy transmission lines is becoming a cause of worry in highly developed networks, because of larger loads and network disruption situations. Voltage instability has been responsible for many significant network failures in recent and past years. Some notable network failure incidences due to voltage instability are given in the following table 2.2 [18].

Table 2.2: Notable Network Failures Due to Voltage Instability [18]–[22]

<b>Incidences</b>	<b>Date</b>
Brazil grid network disturbance	2009
Athens grid network disturbance	2004
Scandinavia grid network disturbance	2003
North-eastern United States grid network disturbance	2003
Idaho (USA) area reactive power deficiency	July 2, 1996
Japanese grid network disturbance	July 23, 1987
French grid network disturbances	January 12, 1987 December 19, 1978
Swedish grid network disturbance	December 27, 1983
Northern Belgium grid network disturbance	August 4, 1982
Florida grid network disturbance	December 28, 1982
New York Power Pool disturbance	September 22, 1970

## **2.5 LVRT Grid Code Requirement for Wind Power**

Low Voltage Ride Through (LVRT) is a crucial grid code condition that needs to be maintained strictly. In order to comply with the modern grid code standards, 90 percent of the voltage must be restored to pre-fault levels in 1500 milliseconds or 1.5 seconds after the fault [23]. Moreover, in the event of grid failures or other network disturbances, wind turbines are expected to inject the maximum required reactive power into the power



grid to maintain the grid voltage stable [24]–[28]. The regulation of voltage is an essential function that is provided by reactive power. Active power cannot be delivered if the voltage on the system is not high enough. The voltage levels that are required for active power to do useful work are often supplied by reactive power. During fault or network disturbance situation, active power curtailment need to be done so that maximum reactive power can be injected to the grid and restore the voltage level. Figure 2.4 shows the LVRT requirements for wind power. As indicated in figure 1, the voltage drop must be within the permitted limit of the RMS value and the time interval are likewise within the specified period [29].

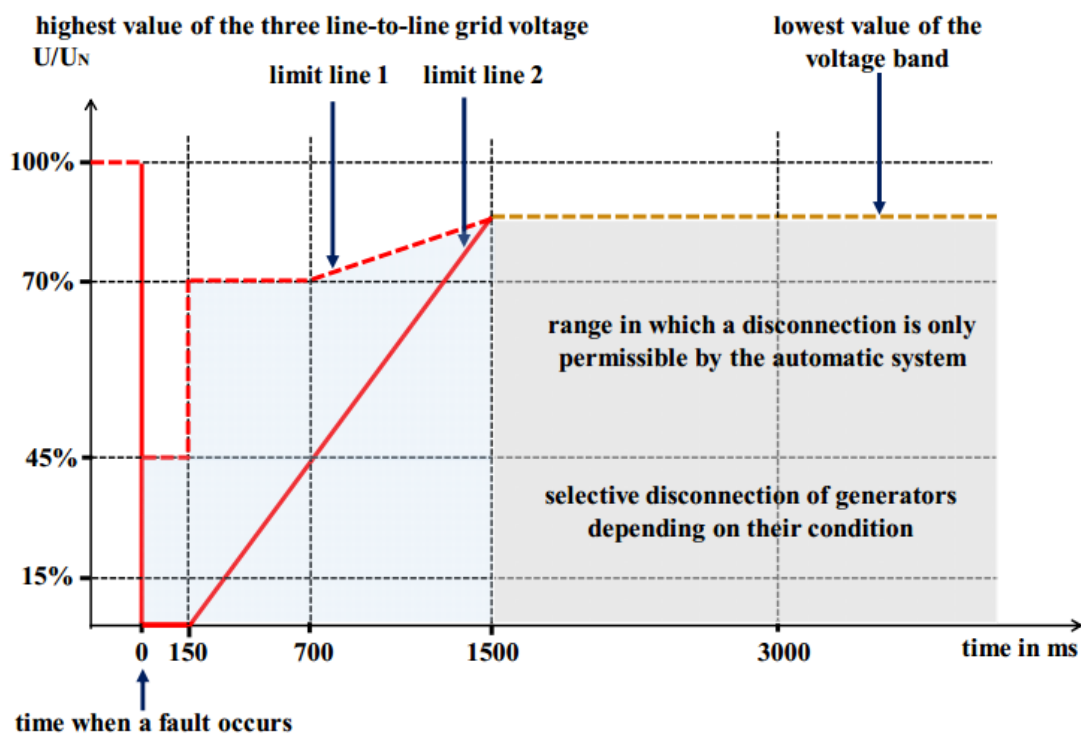


Figure 2.4: Requirement of LVRT for wind farm [29]–[31].

## 2.6 Strategies to Augment LVRT of Wind Farm

Various control strategies have been followed to augment the LVRT or FRT functionality. The present research shows that different authors investigated the issues and proposed various control algorithms to enhance the LVRT functionality.

[32] has discussed a combined approach of fixed and varying speed wind turbine technologies to enhance the LVRT capabilities. Due to insufficient reactive power supply, fixed speed wind turbines can not augment the FRT capabilities which lead to grid instability.

Besides, the variable speed wind turbine technology has inherent LVRT functionality, but it is expensive due to the power electronics converter. Thus, a combined approach of small-scale varying speed wind turbine along with large-scale fixed speed wind turbine might be an efficient solution. For that, a new fuzzy logic-based optimized controller has been introduced at the rotor side of the system. The intended control strategy is also verified using PSCAD simulation tools and transient stability of the whole system is also ensured during network disturbance situations.

[33] has proposed a modified PI controller which is based on Elephant Herding Algorithm (EHA) to provide LVRT enhancement. This optimized controller maintains the voltage regulation at the Point of Connection (POC) to the grid and provides stability in the grid. Authors have also presented optimization techniques by comparing their algorithm with Particle Swarm Optimization (PSO) and Cuckoo Search Optimization (CSO). By applying the disturbances to the system, EHA based optimized PI controller outperforms other mentioned algorithms to augment LVRT capabilities. Besides proposed optimization technique has been used to implement it in the practical system to verify the system performance.

[34] has introduced Salp Swarm Algorithm (SSA) based optimal controller for the grid-tied PV system. SSA is established to tune the PV controller in terms of settling time, percentage overshoots/undershoots and steady-state error of voltage regulation which eventually enhance the LVRT criteria. The authors have also tested the SSA-based optimal controller under various fault conditions and compared the effectiveness of the controller with the functional results of the PV system.

[35] has suggested a coordinated control approach to enhance both the LVRT and the frequency stability of the grid. A novel Battery Storage System (BSS) has been proposed with a modified cascaded PI controller for LVRT enhancement and a droop-based controller for frequency stability. With a coordinated control strategy, BSS ensures the reactive and active power adjustment during transient and dynamic periods respectively. The authors also validated the model by taking into consideration of most severe 3LG fault and actual wind speed data in real-time to analyse LVRT and frequency stability issues. This coordinated control strategy is a novel approach that has a good prospect of enhancing the LVRT and frequency stability at the same time.

The Proportional plus Integral (PI) control is termed as one of the most extensively utilized controller for Voltage Source Converter (VSC). To increase the overall performance of Off-shore Wind Farm (OWF), the novel hybrid optimisation based on CSO and Grey Wolf Optimiser (GWO) method is employed in [36] to design and modify the PI controllers' settings.

Sophisticated control schemes developed by different authors fine-tune the power conversion system but the time and the lengthy training process of such control scheme depends extensively on the experience of the designer [37]. Hence, [38] has used the Taguchi method, an existing optimization technique that is used extensively to solve different problems in electrical power systems. The authors successfully used the Taguchi approach to fine-tune four PI controllers considering the several design variables simultaneously in a cascaded arrangement.

A method to voltage stability analysis considering the IEEE 14-bus, employing multiple approaches is described in [39]. Flexible Alternating Current Transmission System (FACTS) devices, such as Static Synchronous Compensators (STATCOMs) and Static Var Compensators (SVCs) are employed as reactive power compensators in this work to keep the weak bus voltage magnitudes within acceptable ranges. It has been indicated that STATCOMs outperform SVCs in terms of improving voltage stability [39].

## **2.7 Grid Code Criteria of Frequency Operating range**

Different countries follow different grid code requirements due to the generation and network operation criteria. Grid Code requirements were first designed based on the operating characteristics of traditional fossil-fuelled power plants, but have subsequently been adapted to enable more diverse production types to connect to the power network, such as wind, solar power generation etc. It is also important to note that national regulatory frameworks constantly change and revise the grid code.

According to grid code criteria, the normal frequency range is very tight which is around 49.50 Hz to 50.50 Hz in Great Britain, Germany, France and many other countries. Few countries follow more strict rules to maintain the range of frequency. The normal

frequency range of China, Australia and Ireland is 49.80 Hz – 50.20 Hz, 49.75 Hz – 50.25 Hz and 49.80 Hz – 50.20 Hz respectively [40]. However, there is a relaxation of the Transient frequency range in grid code which indicates that, under the permitted frequency oscillating range, wind farms need to be connected to the grid and adjust active power to restore normal frequency [41]. A wind farm can only be separated from the grid if it is out of the transient frequency range. To restore the normal frequency range, different control strategies (i.e. droop controller, fuzzy logic controller, etc.) are adopted which ensures frequency stability in the grid. Most of the national transmission grids that use 50 Hz as the nominal frequency consider transient frequency ranges between 47.00 Hz to 52.00 Hz. A few countries (i.e. China, Australia etc.) follow different frequency intervals because of their robust power systems. Below in table 2.3, is the summary of the normal and transient frequency range of different countries [40].

Table 2.3: Normal and transient frequency range of different countries [40]

<b>Country</b>	<b>Normal Frequency Range</b>	<b>Transient Frequency Range</b>
Great Britain	49.50 Hz – 50.50 Hz	47.00 Hz – 52.00 Hz
Ireland	49.80 Hz – 50.20 Hz	47.00 Hz – 52.00 Hz
Germany	49.50 Hz – 50.50 Hz	47.00 Hz – 52.00 Hz
France	49.50 Hz – 50.50 Hz	47.00 Hz – 52.00 Hz
Australia	49.75 Hz – 50.25 Hz	47.00 Hz – 52 Hz/55 Hz
China	49.80 Hz – 50.20 Hz	48.00 Hz – 51.00 Hz

## 2.8 Hybridization of Wind Turbine System

The most frequently operated wind turbine uses SCIG which is a fixed speed machine. SCIG is simple to build, durable and cost-effective machine which has no LVRT capabilities in the event of a system failure. LVRT is the most important grid code criteria which needs to be maintained strictly. Usually, reactive power is supplied by a capacitor bank, but the capacitor bank of the SCIG can not provide enough reactive power during fault or network disturbance situations which failed the LVRT capabilities of the grid. So, an ideal option could be the hybridization of wind farms by installing a low-capacity DFIG wind turbine with a higher capacity SCIG wind turbine. Thus, cost optimization, as well as LVRT augmentation could be served.

Other hardware-based auxiliary control strategies like Flexible AC Transmissions (FACTS) devices including Static Var Compensator (SVC), Static Synchronous Compensator (STATCOM), Superconducting, Energy Capacitor System (ECS), Thyristor-Controlled Series Capacitor (TCSC) etc. have been integrated with the SCIG. However, the cost of integrating such devices is very high [42].

Among the two kinds of varying speed wind turbine technology, DFIG has the most significant worldwide market share because of its many benefits. These benefits include a lower converter rating, flexible control, lightweight, high efficiency, output strength, superior speed control and independent control to manage both active and reactive power. Additionally, permanent magnet synchronous generators (PMSG) employ full-scale power electronic converters, whereas DFIG-based wind turbine technology employs a partial rating converter. The benefit of DFIG-based WT is that it only requires a fractional power size converter which is around 20% to 30% of the rated generator power to control the system across its entire operating range. The reason for the low-rated power rating converter is that it only manages the rotor 'slip' power [43], [44]. Besides, PMSG based wind farms are highly expensive than the DFIG due to the existence of full rated power converters.

Hence, a good approach is the hybrid installation of a small-scale variable speed-based DFIG machine, including a large-scale fixed speed-based SCIG machine. As traditional SCIG based wind turbine technology can not provide enough reactive power supply thus hybrid installation of DFIG including SCIG is an effective solution to stabilize SCIG with the support of reactive power supply from DFIG. As a result, it is possible to assure the LVRT capability and stability of SCIG at a cheaper cost. However, this technique necessitates a large number of storage components, making the system more complicated and raising the cost. It is also notable that few intelligent control techniques (i.e. fuzzy logic, model predictive controller, etc.) are also employed in the rotor and grid side of the DFIG to improve LVRT functionality. Although the LVRT augmentation can be improved, the computational obligation for employing these intelligent controllers is very high. Furthermore, the success of employing such an intelligent control algorithm mainly depends upon the experience of the designer. Besides, some hardware-based auxiliary circuitry (i.e.

crowbar circuit, bridge type fault current control, STATCOM, etc.) has also been employed to augment the LVRT functionality. However, the cost and complexity are always important factors for integrating the auxiliary circuitry [42].

## **2.9 Chapter Summary**

In this chapter, a complete study of the literature has been undertaken in order to identify the existing research developments in the subject of integrating wind energy into the grid. This study has been carried out with the purpose of providing an overview of the topic. In addition, statistical data from the most recent years has been provided in order to get a better insight of the potential of wind energy and the role that it will play in the overall energy production. This chapter also explores the environmental consequences of different fossil fuels and renewable energy sources to better understand the impact of CO<sub>2</sub> emissions.



# 3 Modelling of Wind Turbine

This chapter aims to present a system model of the wind turbine and various characteristics curves related to the turbine. First, different types of wind energy conversion topologies are discussed. Later, an overview of wind turbine components, details of extracted power, drive train model and pitch controller concepts have been illustrated for varying speed turbine systems. Finally, the detailed model of DFIG wind turbine has been presented.

## 3.1 Topology of Wind Energy Technology

The most important component of the turbine system is the generator machine. Wind turbine topology is usually based on fixed or variable speed generators. Based on the topology two types of topologies are usually considered. Squirrel Cage Induction Generator (SCIG) is a fixed-speed turbine because it runs at a constant speed. Doubly-Fed Induction Generator (DFIG) and Permanent Magnet Synchronous Generator (PMSG) are two varying speed turbine generator technologies. In comparison to fixed-speed machines which are constructed for one specific wind speed, variable-speed wind generators capture more energy due to the precise control of the rotational speed according to the wind speed. A variable speed wind turbine machine employs power electronics converter which is expensive and consists of sensitive electronic equipment. Besides, PMSG requires full-scale power converters which is more costly than partially rated power semiconductor converters of DFIG [45], [46]. Different types of wind turbine technologies have been presented in figure 3.1 – 3.3.

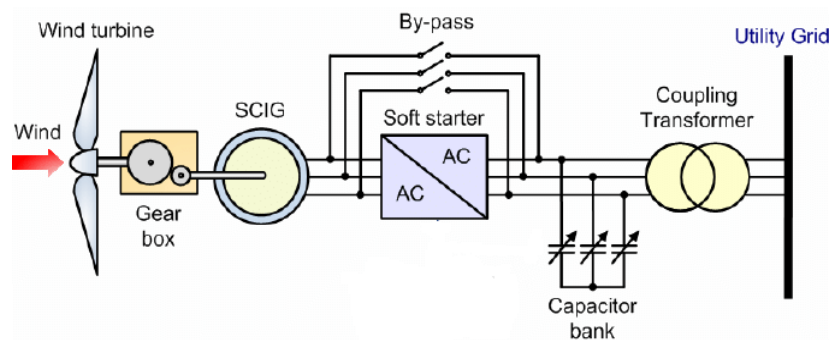


Figure 3.1: Topology of fixed speed (SCIG) turbine technology [47].



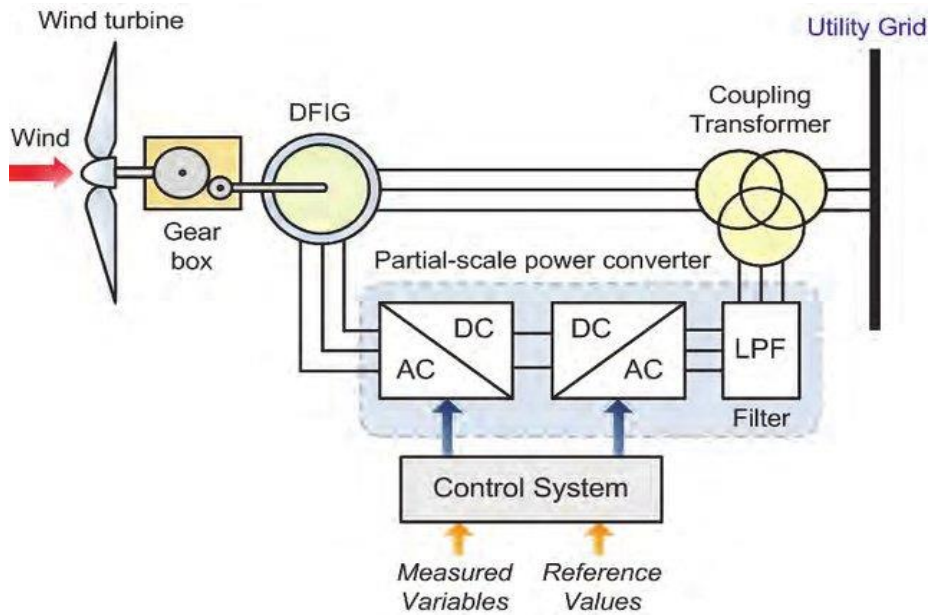


Figure 3.2: Topology of variable speed (DFIG) turbine technology [48].

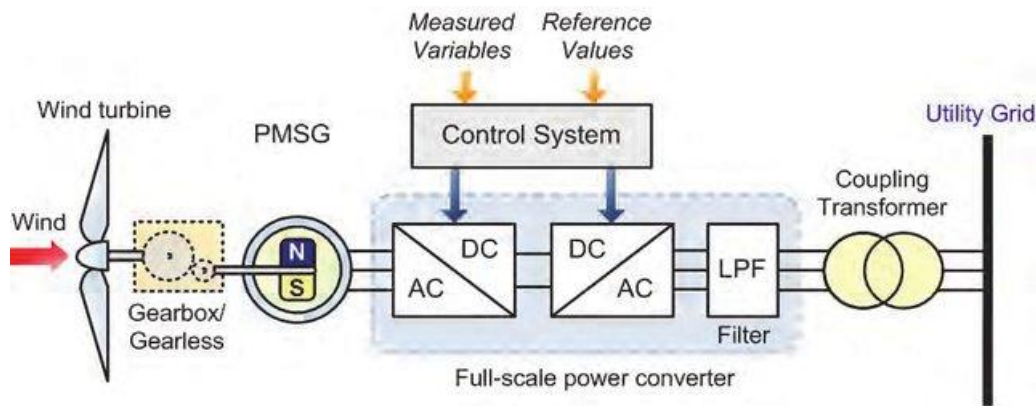


Figure 3.3: Topology of variable speed (PMSG) turbine technology [47].

### 3.2 Wind Turbine System Components

The turbine of a wind power system is a rotational machine that takes part in the conversion process of the wind energy into electrical energy. Present wind turbine generators are designed as a system with a horizontal axis rotational machine, generator, gearbox and rotor brake situated in the nacelle over the tower [49]. The turbine absorbs the produced rotational kinetic energy and uses it to drive the generator. The nacelle is supported by the tower, which also houses the electrical conduits and yaw drive.

As depicted in figure 3.4, a wind turbine system includes some major components which take part in the energy conversion process. Most wind turbines typically have three

blades. The blades revolve because of the wind blowing across them. An anemometer is usually employed to determine the speed of the wind. Later, the anemometer data is sent to the controller for further control process. The wind vane has been employed to detect the direction of the wind and interacts with the yaw drive to properly align the turbine with the direction of the wind. As the direction of wind varies, the yaw drive is employed to maintain the rotor towards the wind direction [50], [51].

The high and low-speed shafts, gearbox, turbine and generator rotational mass constitute the drive train model. The turbine's output mechanical power transfers to the generator rotor in the drive train process. The horizontal-axis turbine's rotor spins as the wind impacts it. The low-speed shaft delivers energy to the gearbox, which increases the rotational speed of the high-speed shaft. The generator spins due to the high-speed shaft, which generates electricity. The low and high-speed shaft equip with aerodynamic and mechanical brakes. In the event of malfunction of the aerodynamic brake, the emergency mechanical brake comes into operation [52].

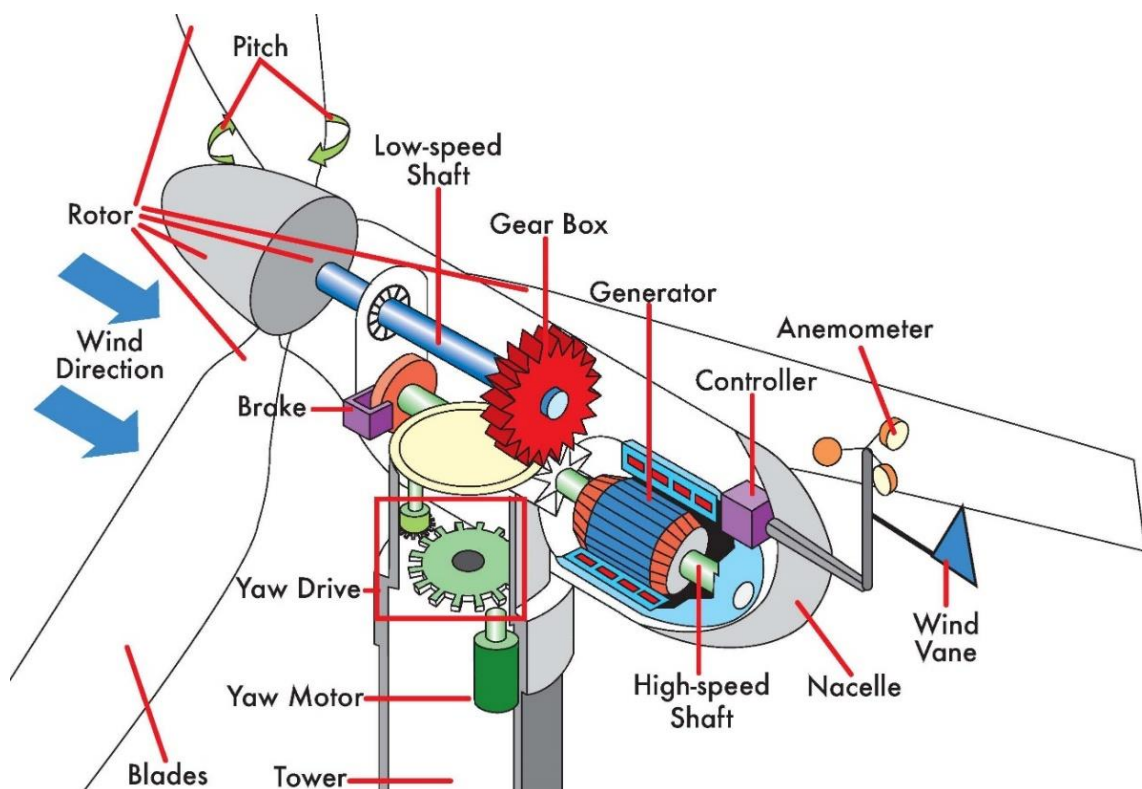


Figure 3.4: Major Components of a Wind Turbine [53].

Typically, the generator provides electricity at a lower voltage level and a step-up voltage transformer is utilized to raise the voltage level according to the grid level voltage. To reduce losses, the transformer might be installed in the nacelle or near the bottom of the hub tower [52].

### 3.3 Extracted Output Power of the Wind Turbine

The turbine wind's extracted output power can be defined as [17]

$$P_w = \frac{1}{2} \rho \pi R^2 U_w^3 C_p(\lambda, \beta) \quad (3.1)$$

Where,

$P_w$  = extracted wind output power in Watt,

$\rho$  = density of air in Kg/m<sup>3</sup>,

$R$  = blade radius in meters or (m)

$U_w$  = speed of wind in m/s

$C_p$  = wind power coefficient

$\lambda$  = tip speed ratio or TSR and

$\beta$  = pitch angles in degrees or (°)

$\lambda$  and  $\beta$  of the turbine determine the value of the  $C_p$ . The wind power coefficient is calculated using the [17]

$$C_p(\lambda, \beta) = c_1 \left( \frac{c_2}{\lambda_i} - c_3 \beta - c_4 \right) e^{-\frac{c_5}{\lambda_i}} + c_6 \lambda \quad (3.2)$$

$$\frac{1}{\lambda_i} = \frac{1}{\lambda - 0.08\beta} - \frac{0.035}{\beta^3 + 1} \quad (3.3)$$

$$\lambda = \frac{\omega_r R}{V_w} \quad (3.4)$$

$$T_w = \frac{P_w}{\omega_r} \quad (3.5)$$

Where,

$T_w$  = torque of the turbine in N/m,

$\omega_r$  = rotational speed in rad/s.

The turbine's characteristic coefficients are  $c_1 = 0.5176$ ,  $c_2 = 116$ ,  $c_3 = 0.4$ ,  $c_4 = 5$ ,  $c_5 = 21$  and  $c_6 = 0.0068$  [18].

For several values of pitch angles  $\beta$ , the  $C_p$  vs  $\lambda$  characteristics have been illustrated as shown in figure 3.5. When pitch angle,  $\beta = 0^\circ$ , the optimum values of power coefficient ( $C_{p\_opt}$ ) and TSR ( $\lambda_{opt}$ ) are found 0.48 and 8.1 respectively.

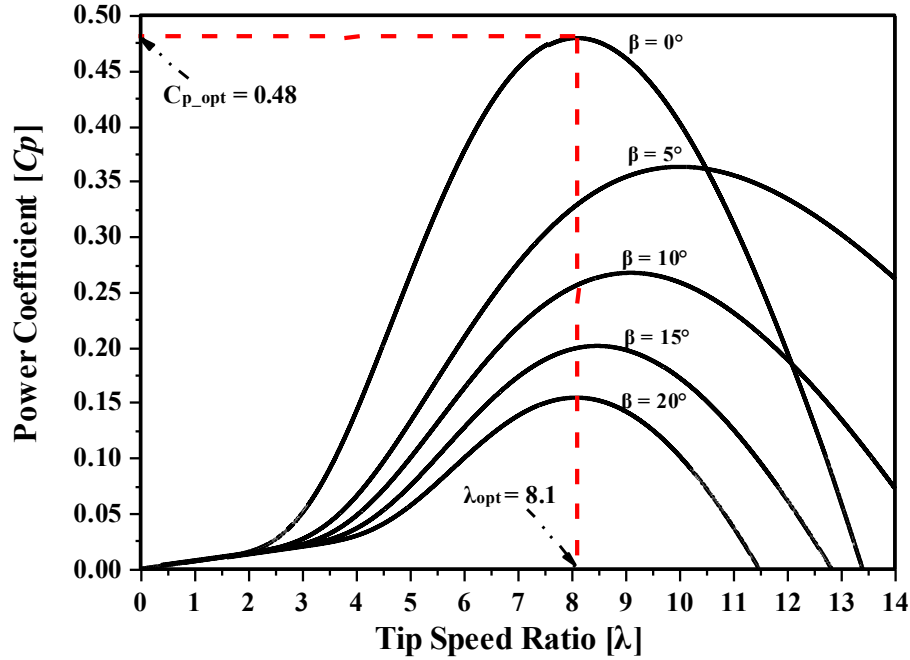


Figure 3.5: Wind power coefficient ( $C_p$ ) vs TSR ( $\lambda$ ) characteristics curve [42].

The rotational speed,  $\omega_r$  in VSWT is set to adopt the Maximum Power Point Tracking (MPPT). The MPPT curve for DFIG based wind turbine has been depicted in figure 3.6. According to the available wind speed, the MPPT curve is separated into four functioning areas [54]:

- Point A to B (minimum speed zone): The DFIG speed in this location is around 70 percent of the synchronous speed.
- Point B to C (optimal speed zone): This working zone considers DFIG's most effective operation region until the maximum speed is reached which is about 1.2 pu or 120 percent of the synchronous speed.
- Point C to D (maximum speed zone): The generator speed achieves its maximum speed in this working zone and the rotor side converter of DFIG sets to maintain the speed at its maximum speed.
- Beyond point D (restricted/overspeed zone): Due to the increased inbound wind speed, mechanical power generation may surpass the rated power at this operating position. As a result, the pitch controller is turned on to keep the rated turbine speed.

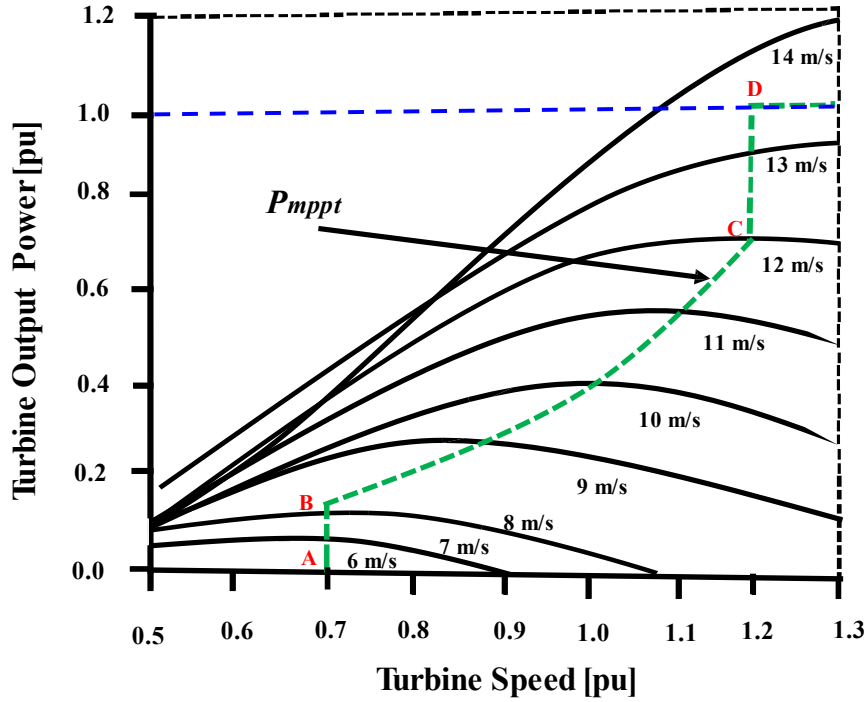


Figure 3.6: MPPT curve for DFIG based wind turbine [55].

### 3.4 Modelling Drive Train System

The wind turbine's rotational mass is made up of blades with a rotor hub and a generator shaft. Drive train system could be developed utilizing single lumped mass or 2-mass model. When studying the interaction between wind turbines with grid systems, a single lumped mass model is enough for the purpose of time efficacy [52]. The following equation [56] has been used to model the single mass drive train system:

$$\frac{d\omega_r}{dt} = \frac{T_e - T_m}{J_{eq}} - \frac{B_m}{J_{eq}} \omega_r \quad (3.6)$$

Where,

$\omega_r$  = rotational speed in rad/s,

$B_m$  = damping or friction co-efficient in Nm/s,

$T_m$  = torque (mechanical) in Nm,

$T_e$  = torque (electromechanical) in Nm and

$J_{eq}$  = rotational equivalent inertia of the generator in  $\text{kgm}^2$ .

The modelling of the single lumped mass drive train system of the turbine is presented in figure 3.7.

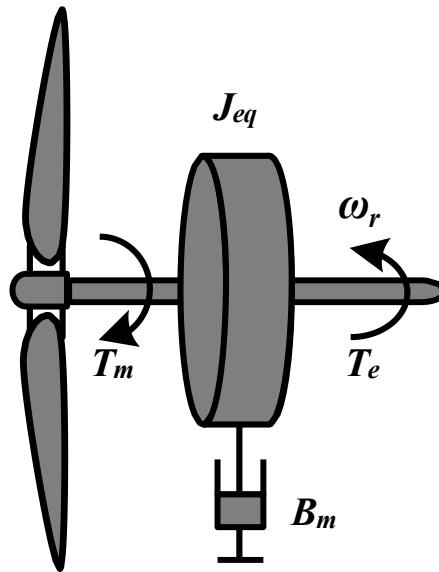


Figure 3.7: Single lumped mass drive train system of the turbine [56].

### 3.5 Controller for Pitch Angle

Wind turbines extract wind power based on the speed of wind; hence the extracted output power of a wind generator is continually fluctuating due to wind speed fluctuations. The controller for the pitch angle as shown in figure 3.8 is used for DFIG to keep the generator's output power below the rated level.

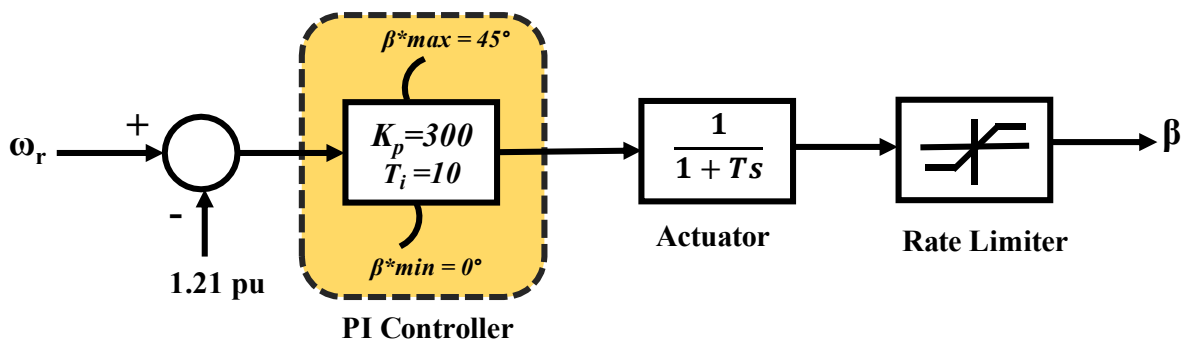


Figure 3.8: DFIG's pitch angle controller.

To manage tracking error, a traditional PI controller is employed where  $K_p$  and  $T_i$  are the proportional and integral constant respectively. The pitch control actuator is comprised of a 1<sup>st</sup> order transfer function, where  $T$  is the time constant. The pitch controller is employed

in a varying speed wind turbine to maintain the DFIG's rotational speed below its rated value ( $\omega_r = 1.21$  pu).

### 3.6 Induction Machine Characteristics

Based on the required operation, an induction machine can function as a generator or motor. When the shaft of an induction machine rotates faster than the synchronous speed, it works as a generator. Under the generator mode, an induction machine operates in the negative torque region hence, giving negative slip.

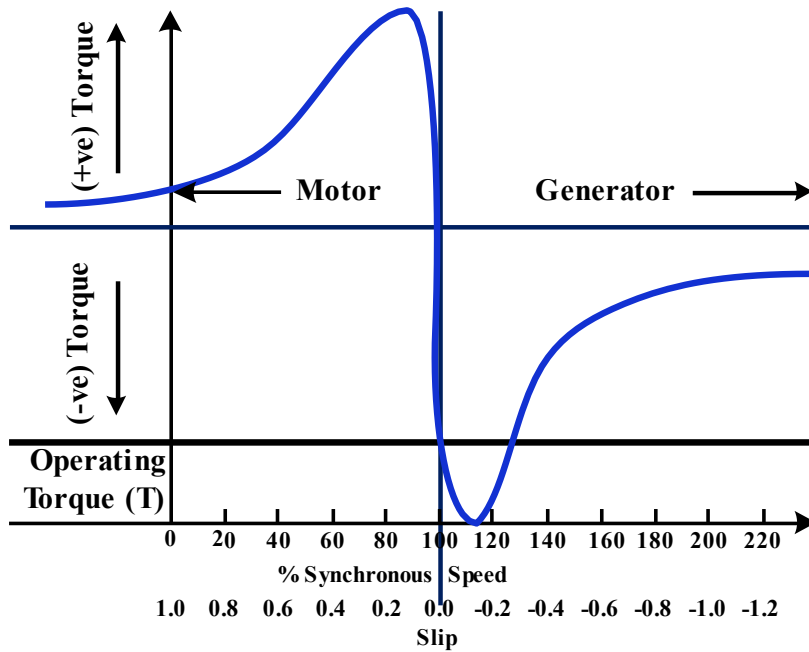


Figure 3.9: Induction machine's Torque-slip curve [57].

As depicted in figure 3.9 an induction machine works as a generator if it is governed by a prime mover at larger than 100 percent of the synchronous speed [57].

### 3.7 WRIG Model

DFIG is based on Wound Rotor Induction Generator (WRIG) machine. Hence, the differential equations of WRIG model in the “d” and “q” axis rotating reference frame are expressed as [42]:

$$V_{sd} = R_s \cdot i_{sd} + \frac{d\phi_{sd}}{dt} - \omega_s \cdot \phi_{sq} \tag{3.7}$$

$$V_{sq} = R_s \cdot i_{sq} + \frac{d\phi_{sq}}{dt} + \omega_s \cdot \phi_{sd} \tag{3.8}$$

$$V_{rd} = R_r \cdot i_{rd} + \frac{d\phi_{rd}}{dt} - \omega_r \cdot \phi_{rq} \tag{3.9}$$

$$V_{rq} = R_r \cdot i_{rq} + \frac{d\varphi_{rq}}{dt} + \omega_r \cdot \varphi_{rd} \quad (3.10)$$

Here,

$R_s$  = stator winding resistance ( $\Omega$ )

$R_r$  = rotor winding resistance ( $\Omega$ )

$L_m$  = mutual inductance (henry)

$\omega_r$  and  $\omega_s$  are rotor and stator angular frequency (rad/s) respectively

$V_{rd}$ ,  $V_{rq}$ ,  $V_{sd}$  and  $V_{sq}$  are “d” and “q” axis rotor and stator voltages (volt) respectively

$i_{rd}$ ,  $i_{rq}$ ,  $i_{sd}$  and  $i_{sq}$  are “d” and “q” axis rotor and stator current (ampere) respectively

$\varphi_{rd}$ ,  $\varphi_{rq}$ ,  $\varphi_{sd}$  and  $\varphi_{sq}$  are “d” and “q” axis rotor and stator flux linkage (weber) respectively

The flux linkages of stator and rotor can be denoted as [42]

$$\varphi_{sd} = L_{st} \cdot i_{sd} + L_m \cdot i_{rd} \quad (3.11)$$

$$\varphi_{sq} = L_{st} \cdot i_{sq} + L_m \cdot i_{rq} \quad (3.12)$$

$$\varphi_{rd} = L_{rt} \cdot i_{rd} + L_m \cdot i_{sd} \quad (3.13)$$

$$\varphi_{rq} = L_{rt} \cdot i_{rq} + L_m \cdot i_{sq} \quad (3.14)$$

Here,

$L_m$  is represented as mutual inductance.

$L_{rt}$  and  $L_{st}$  are the self-inductance of rotor and stator winding respectively.

PSCAD EMTDC® v4.5 has a built-in WRIG model [58], which has been used in this thesis work for power system model and further analysis.

### 3.8 VSWT-DFIG Based Configuration

The VSWT-DFIG arrangement is depicted in Figure 3.10. The model includes an aerodynamically designed wind turbine, a controller for pitch angle, a partially rated power converter based on the semiconductor device and a WRIG generator. The stator of the WRIG is directly linked to the grid system and the rotor of the WRIG is connected to the grid via a partially rated power converter which is rated at 30 percent of the generator rating. The power converter is controlled by the rotor and grid side controller (RSC and



GSC). A DC link circuit is used in between the RSC and GSC. The phase angle,  $\theta_g$  of grid side has been extracted using the Phase-Locked Loop (PLL) block [59].

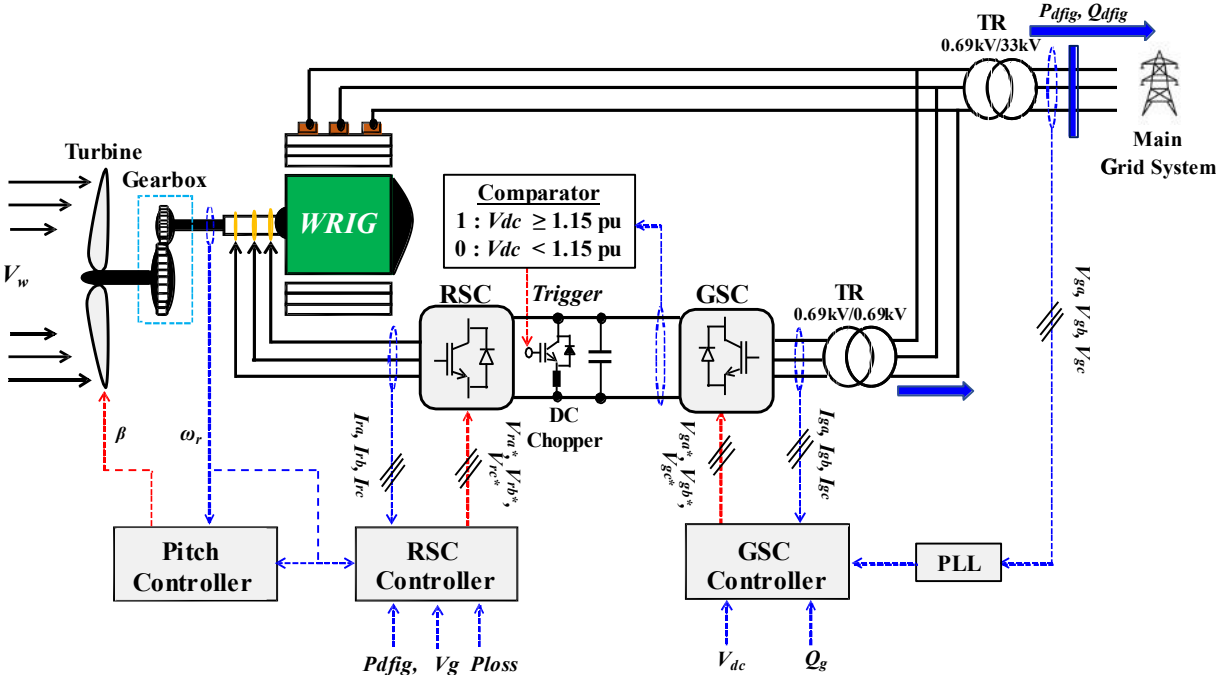


Figure 3.10: Configuration of VSWT-DFIG [59].

### 3.9 Chapter Summary

The purpose of this chapter is to illustrate a system model of the wind turbine as well as various characteristic curves associated with the turbine. Three types of wind energy conversion topologies are first addressed. Later, for varying speed turbine systems, an overview of wind turbine components, extracted power output, drive train model and pitch controller ideas have been shown. Finally, a basic DFIG wind turbine model has been presented.

# 4 DFIG Control Scheme

This chapter aims to present DFIG control schemes including rotor and grid side controllers. To achieve stability during fault or network disturbance situations, modified PI controllers with optimized proportional and integral constant parameters have been used in RSC and GSC. A two-level power converter including a DC link circuit and protection scheme has also been addressed.

## 4.1 Two Level Power Converter

Wind energy applications often use two or three-level converters. In this work, a two-level power converter has been used as shown in figure 4.1. The power circuit of the left and right hand part of the converter is linked by a DC link circuit consisting of switch  $S_c$ , resistor  $R_c$  and capacitor  $C_{dc}$ . The converter is comprised of twelve power electronics switches named  $S_{1r}$ ,  $S_{2r}$ ,  $S_{3r}$ ,  $S_{4r}$ ,  $S_{5r}$  and  $S_{6r}$  for the rotor side and  $S_{1g}$ ,  $S_{2g}$ ,  $S_{3g}$ ,  $S_{4g}$ ,  $S_{5g}$  and  $S_{6g}$  for grid side converter. The gate pulses for controlling the converter are produced using the well-known PWM technique. At the fundamental frequency of the output voltage, a triangular carrier waveform of 3 kHz is compared to a reference sinusoidal waveform [60]. The rotor side converter takes three-phase input voltages ( $V_{ra}$ ,  $V_{rb}$  and  $V_{rc}$ ) and converts them to DC voltage ( $V_{dc}$ ), which is the grid side converter's input voltage, while the grid side converter's output voltages are  $V_{ga}$ ,  $V_{gb}$  and  $V_{gc}$ .

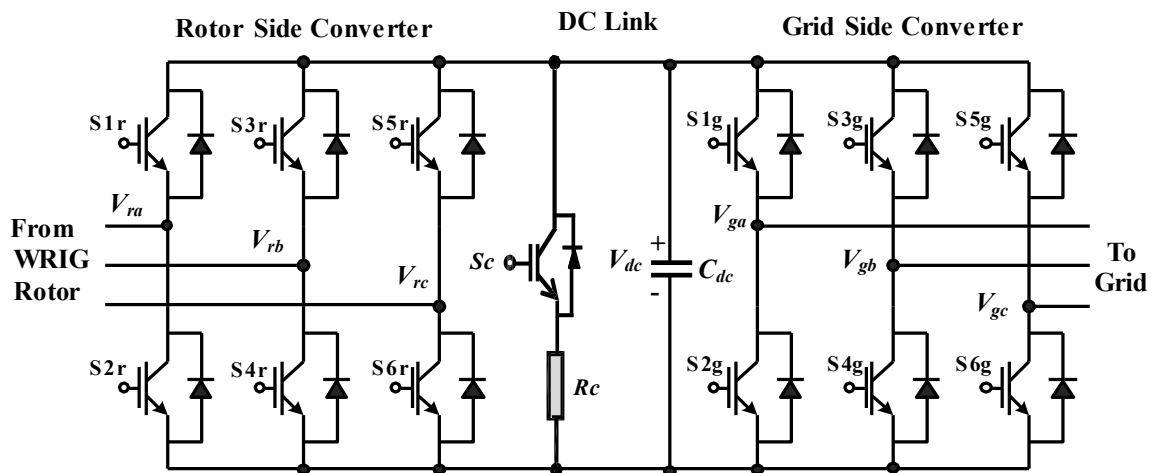


Figure 4.1: Two-level power semiconductor converter

This interconnection has several benefits, including local grid voltage and frequency management and improved power quality in both transient and dynamic operations [55].

## 4.2 DC Link Circuit

The AC/DC rectifier of the RSC side transforms the generator's output to DC power which is sent to the GSC using the common DC link circuit and then supplied to the grid. A capacitor is included in the DC link connection. The capacitor charging and discharging occurs through RSC and GSC currents respectively in the DC link connection. During a fault scenario, the voltage across the DC link connection increases dramatically because of the power imbalance between the generator and the electricity delivered to the grid. The protective strategy is to incorporate a DC chopper into the DC link circuit to avert damage of the power semiconductor converter. The comparator block is used for controlling the DC chopper circuit switch. When in the DC link voltage,  $V_{dc}$  is greater or equal 1.15 pu, the DC chopper protection circuit activates to prevent the damage of the converter. The dynamic behaviour of DC voltage across the capacitor ( $V_{dc}$ ) can be represented by the following equation when power losses in the DC connection are ignored [57]:

$$\frac{dV_{dc}}{dt} = \frac{1}{C_{dc}V_{dc}} (P_r - P_{dc}) \quad (4.1)$$

Where  $C_{dc}$  expresses the DC link capacitor and  $P_{dc}$  is the power delivered to GSC.

## 4.3 Detailed Configuration of DFIG

A detailed configuration of the DFIG including aerodynamic wind turbine model, WRIG generator, IGBT based back-to-back converter, DC link circuit, DC link protection controller, RSC, GSC and other different elements have been presented in figure 4.2. PSCAD EMTDC® v4.5 has a built-in WRIG model [58], which has been used in this work. As indicated in figure 4.2, the stator of the WRIG is directly linked to the power grid system and the WRIG's rotor is tied to the power grid via a partially rated power converter which is rated at 30 percent of the DFIG's rating. The WRIG is governed by the wind turbine, which converts wind energy into electrical energy. The rotor of the WRIG provides the rotational speed ( $\omega_r$ ). The rotor position ( $\Theta_r$ ) is determined from the WRIG rotor. When the turbine's rotational speed surpasses the rated speed, a pitch angle controller comes into

operation to reduce the output power by adapting the pitch blade angle. A transformer is employed to link the GSC to the grid system.

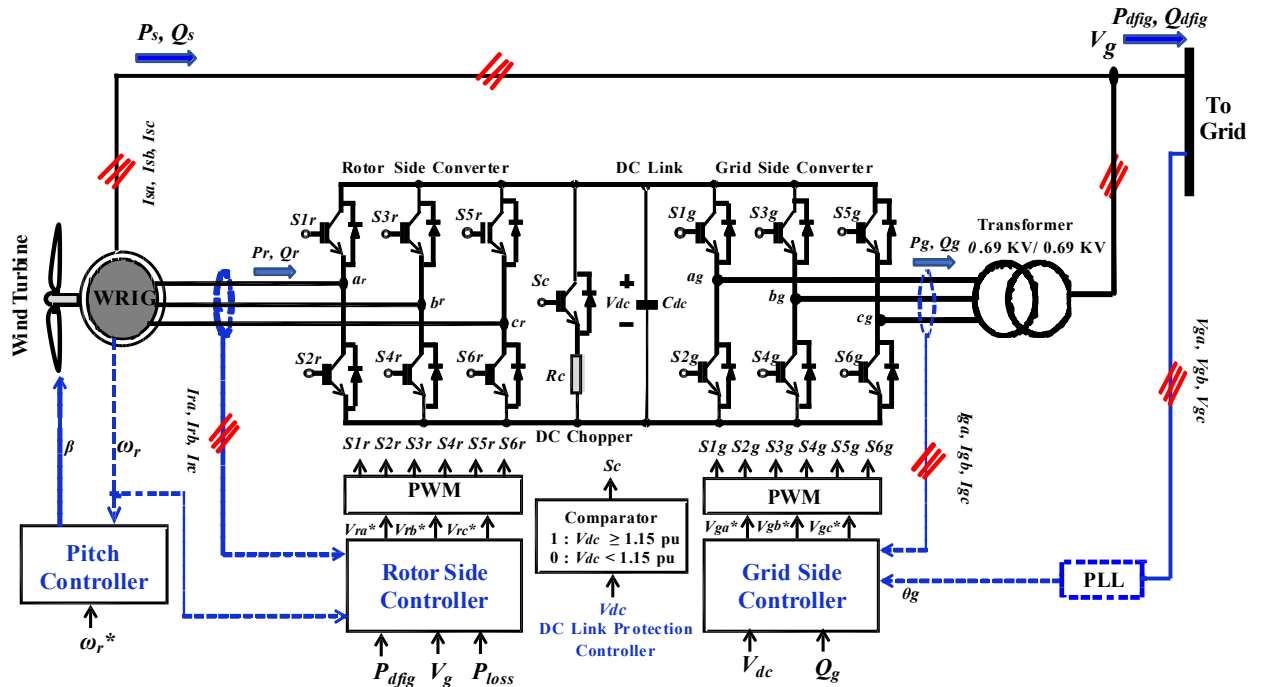


Figure 4.2: Detailed Configuration of DFIG

## 4.4 PI Controller

The Proportional plus Integral (PI) controller is considered the most common and widely used controller for the optimization of power system applications. PI controller consists of proportional ( $K_P$ ) and integral ( $K_I$ ) parameter constants which are tuned to achieve certain objectives. In this work, total eight PI controllers have been utilized to attain the stability of the power system model during fault or network disturbance situations. A schematic diagram of the PI control tuner has been illustrated in figure 4.3.

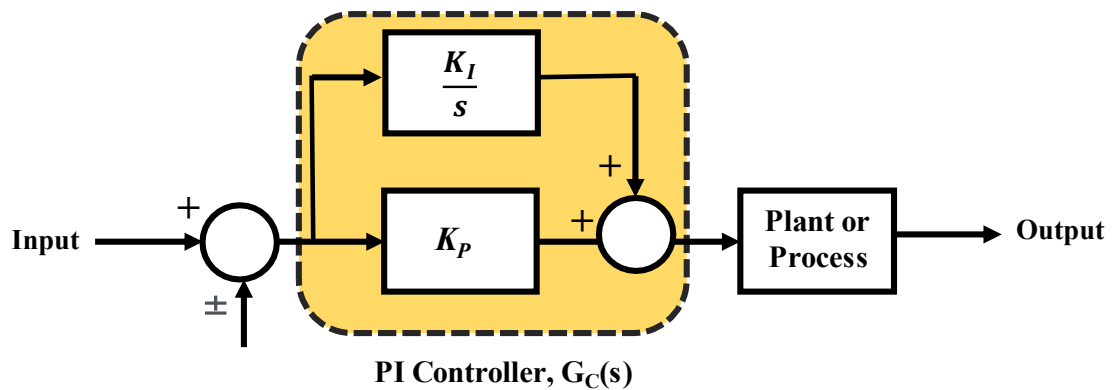


Figure 4.3: Cascaded PI Controller

From figure 4.3, the PI compensator equation can be written as [61]

$$\begin{aligned}G_C(s) &= K_P + \frac{K_I}{s} \\ &= K_p \left(1 + \frac{1}{\frac{K_p}{K_I} s}\right) \\ &= K_p \left(1 + \frac{1}{T_I s}\right)\end{aligned}\tag{4.2}$$

Where,

$\frac{K_P}{K_I}$  is the time constant,  $T_I$ .

$K_P$  is the proportional parameter constant

$K_I$  is the integral parameter constant

$K_P$  and  $K_I$  are tuned in this work experimentally to attain the stability of the power system model during fault or network disturbance situations.

## 4.5 Rotor Side Controller

In this work, four cascaded PI controllers have been used in RSC as depicted in figure 4.4. At RSC, various error signals are compensated using PI controllers. The reference grid voltage ( $V_g^*$ ) is kept at 1.0 pu for maintaining grid code requirements. The active and reactive power provided to the grid is regulated by “q” and “d” axis rotor currents  $I_{rq}$  and  $I_{rd}$  respectively [61].

The comparator block has been employed to adopt the grid code condition for LVRT. Under typical operating condition i.e. grid voltage is greater than 0.9 pu, the active power provided to the power grid maintains active reference power output as stated in equation 4.3. When the grid voltage,  $V_g$  falls below 0.9 pu, the comparator block considers it faults or network disturbance situations and curtails the active power transmission to zero. Thus, the reactive power fed into the power grid can be maximised by managing the power this way.

Based on the experimental technique, the parameters of the PI controllers (PI 1 to PI 4) have been determined. Different values have been explored under various system situations and the values presented in Table 4.1 are ultimately chosen as the optimal values.

Limiters are used to keep the PI controllers' limits within acceptable limits. Thus, reactive power can be effectively fed into the grid assuring LVRT competence in the transient and dynamic state.

Table 4.1: PI controllers optimized parameters at RSC

PI Controllers	$K_P$	$K_I$
PI 1	1	10
PI 2	0.9	8
PI 3	1.5	15
PI 4	0.01	0.05

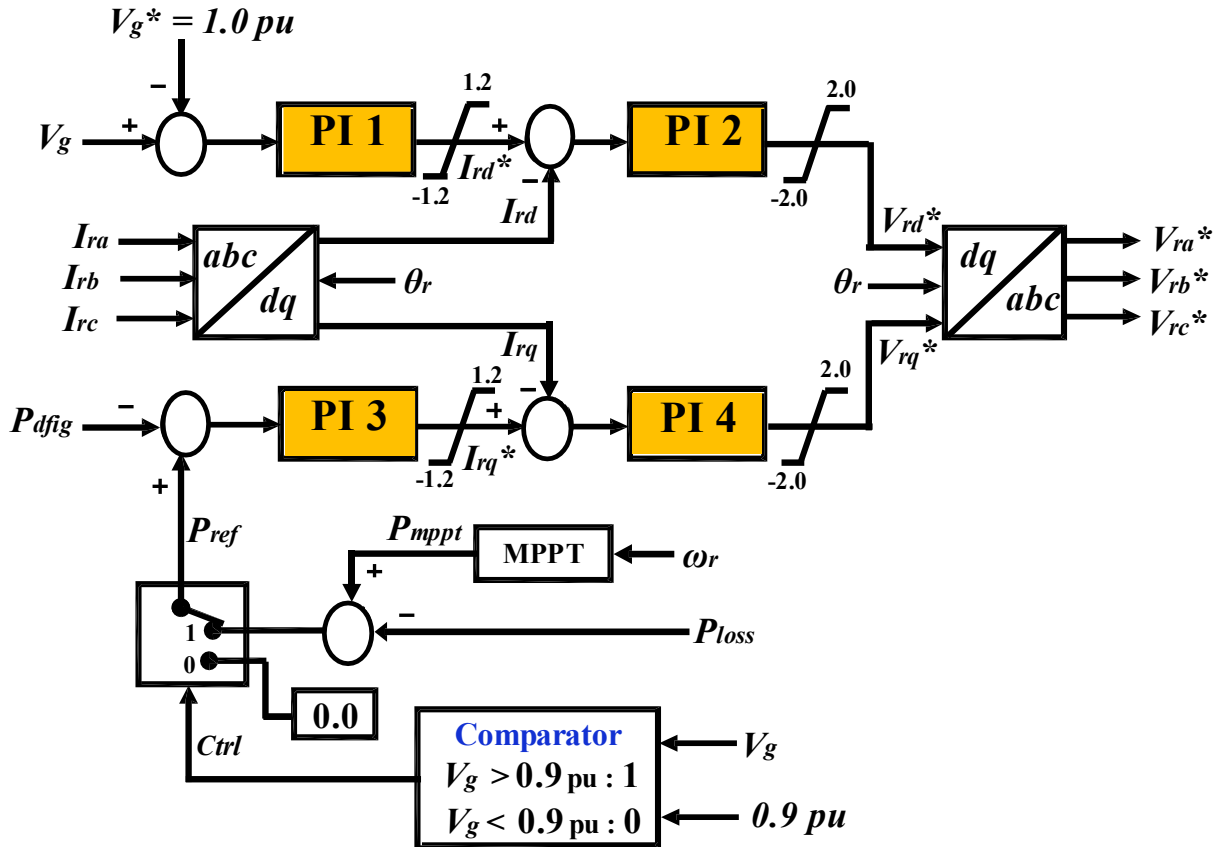


Figure 4.4: Rotor Side Controller of DFIG [32].

The active power reference ( $P_{ref}$ ) has been determined using

$$P_{ref} = P_{mppt} - P_{loss} \quad (4.3)$$

Stator, rotor and turbine losses have been considered in the total losses ( $P_{loss}$ ) as can be seen in figure 4.5.

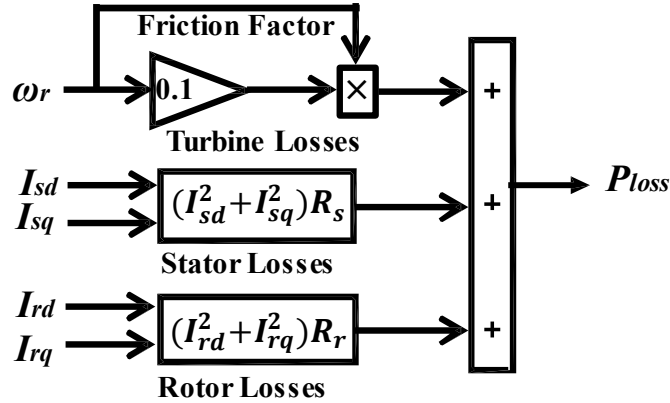


Figure 4.5:  $P_{loss}$  considering stator, rotor and turbine losses [32].

## 4.6 Grid Side Controller

Four cascaded PI controllers have been used in GSC as depicted in figure 4.5. At GSC, various error signals are compensated using PI controllers. The reference reactive power ( $Q_g^*$ ) and reference DC link voltage are kept at zero and 1.0 pu respectively for maintaining grid code requirements. The DC link voltage ( $V_{dc}$ ) and GSC reactive power ( $Q_g$ ) are regulated by q and d axis currents  $I_{gq}$  and  $I_{gd}$  respectively [32], [61].

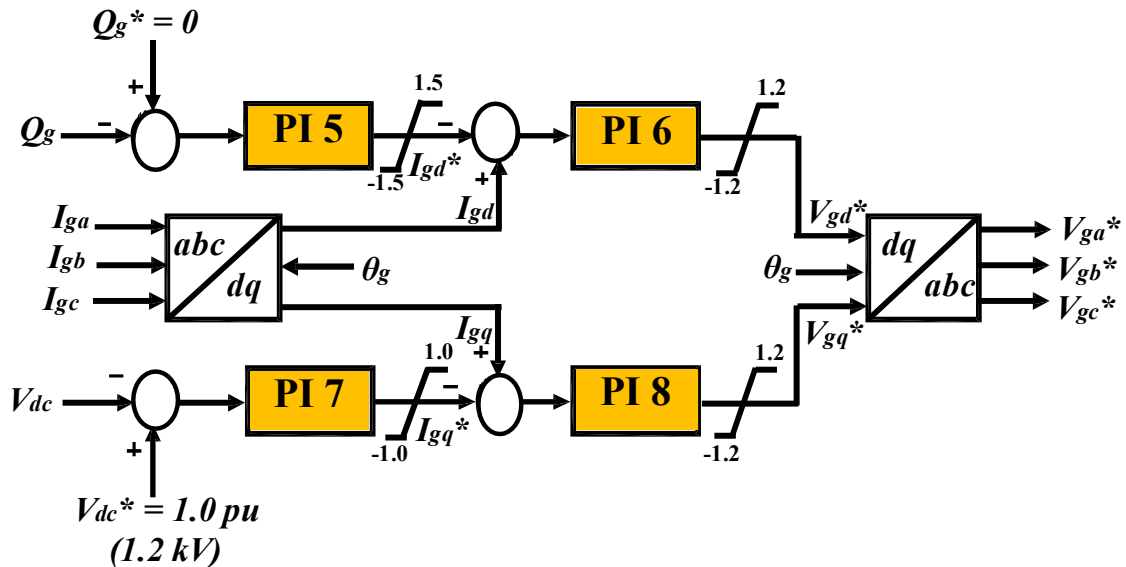


Figure 4.5: Grid Side Controller of DFIG [32].

Based on the experimental technique, the parameter constants of four PI controllers (PI 5 to PI 8) have been determined. Different values have been explored under various system

situations and the values presented in Table 4.2 are ultimately chosen as the optimal values. Limiters are also used to keep the PI controllers' limits within acceptable limits. Thus, reactive power can be effectively fed into the power grid assuring LVRT competence in the transient and dynamic state.

Table 4.2: PI controllers optimized parameters at GSC

<b>PI Controllers</b>	<b>K<sub>P</sub></b>	<b>K<sub>I</sub></b>
PI 5	1	10
PI 6	0.9	8
PI 7	1	10
PI 8	0.01	0.08

## 4.7 Chapter Summary

This chapter presents the DFIG control method which includes rotor and grid side controllers. In RSC and GSC, PI controllers with tuned proportional and integral constant parameters have been employed to ensure stability under fault or network disruption circumstances. In addition to this, a two-level back-to-back converter that consists of a DC link circuit with a protection mechanism has been presented.





# 5 Results and Analysis

This chapter illustrates a complete power system model which is connected to an infinite bus. Different fault scenarios including the most severe fault i.e. 3LG have been considered for the transient stability assessment of the system. Transient stability evaluation has been performed for a very short period and dynamic stability analysis has been considered for a longer duration. For both dynamic and transient cases, a comprehensive analysis has been performed.

## 5.1 Power System Model

Figure 5.1 depicts the complete schematic model of the power system considered in this work. DFIG rated at 20 MVA is linked to an infinite bus by means of a 0.69KV/6.6 KV step-up transformer and a short dual transmission line. The dual transmission line consists of two circuit breakers (CB) in each line, so that, if an adverse situation occurs during a fault or network disturbance situation, it can be isolated from the power system.

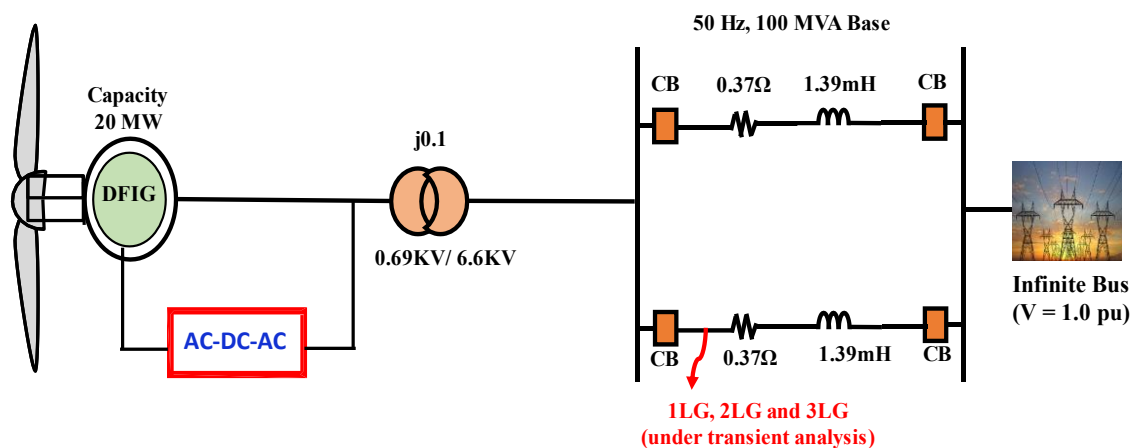


Figure 5.1: A complete schematic of the power system model

The transmission line parameters are shown in figure 5.1 in the form of resistance and inductance. The rated frequency of the system is 50 Hz, while the system's base power is 100 MVA. Table 5.1 lists the DFIG's required parameters.

Table 5.1: DFIG's parameters

<b>WRIG</b>	$P_{base}$ [Rated Power]	20 [MVA]
	$V_{base}$ [Rated Voltage]	0.69 [kV]
	$R_s$ [Stator Resistance]	0.007 [pu]
	$R_r$ [Wound Rotor Resistance]	0.005 [pu]
	$X_{md}$ [Magnetizing Inductance]	2.9 [pu]
	$X_a$ [Stator Leakage Inductance]	0.171 [pu]
	$X_{kd1}$ [Wound Rotor Leakage Inductance]	0.156 [pu]

## 5.2 Dynamic Stability Performance Analysis

Dynamic stability performance analysis has been conducted by utilizing actual wind speed data from Hokkaido island in Japan [62] as shown in figure 5.2. The schematic model power system which is depicted in figure 5.1 used in this work. Dynamic analysis is performed for a long duration (300 sec) with the varying wind speed data. From figure 5.2, it has been observed that the wind speed varies from 8.6 m/s to 13 m/s for the considered period.

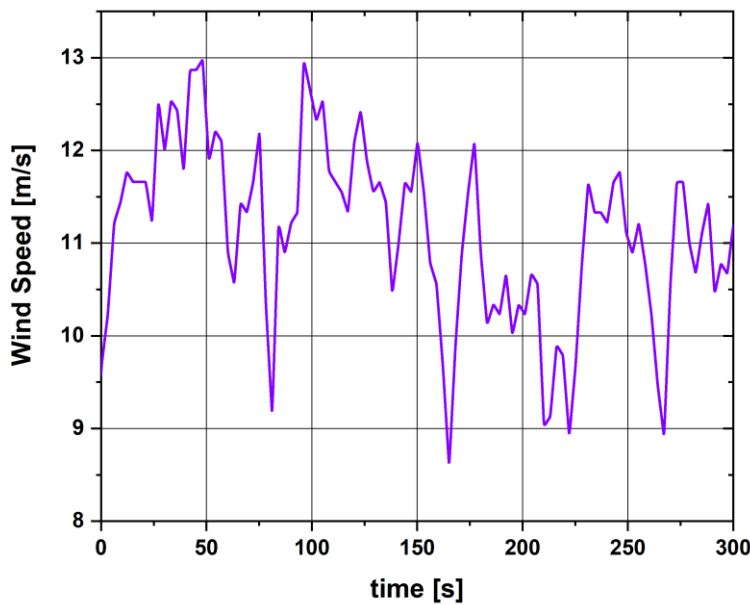


Figure 5.2: Variable wind speed data [62].

The DFIG's wind speed at rated condition is considered 12.5 m/s. The pitch angle response of the wind turbine is shown in figure 5.3, which shows that the pitch angle controller comes into operation when the DFIG's wind speed surpasses the rated condition of 12.5 m/s (as figure 5.2).

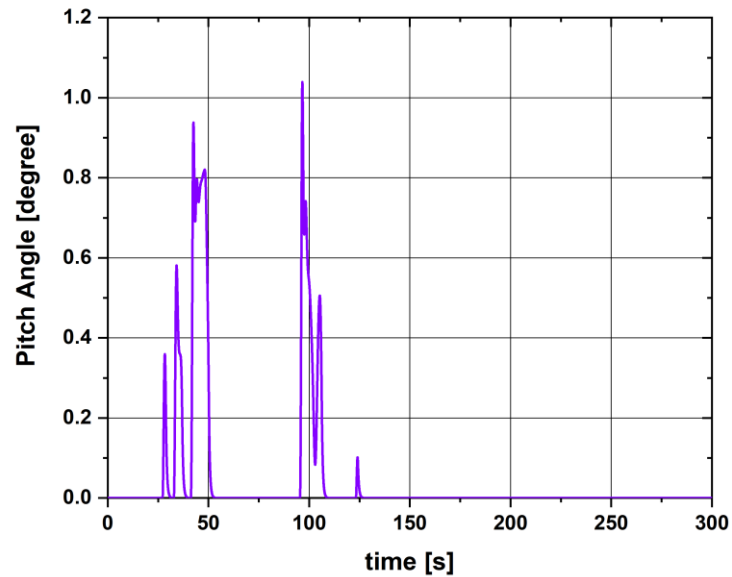


Figure 5.3: Pitch angle response

Active power output both in MW and per unit has been shown in figures 5.4 and 5.5 respectively.

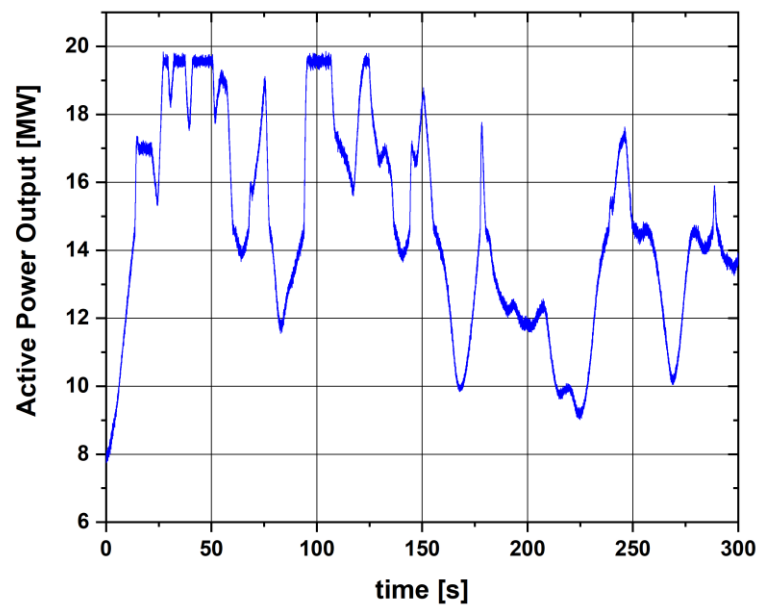


Figure 5.4: Active power output in MW

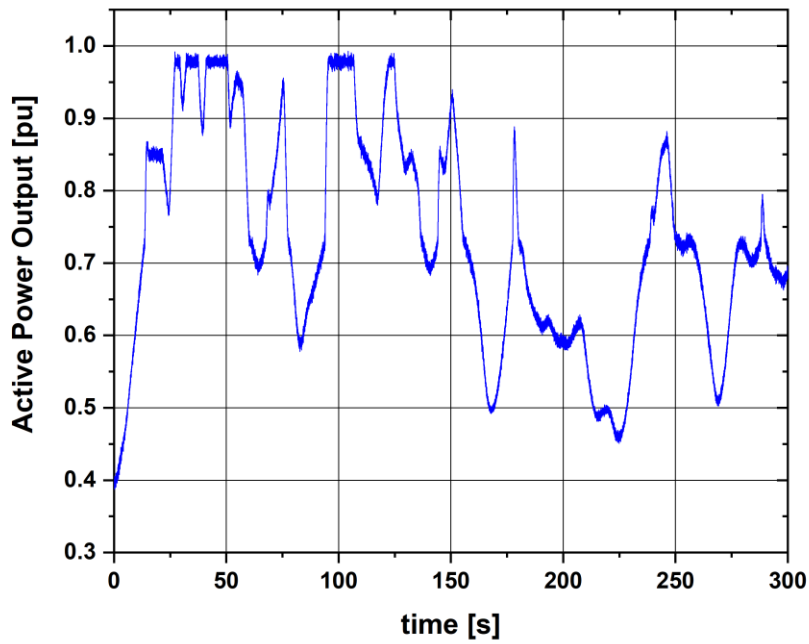


Figure 5.5: Active power output in per unit

Active power generation of DFIG varies over time due to the variable wind speed. The maximum power output can be achieved near 20 MW or 1.0 pu during the wind speed at rated condition of 12.5 m/s.

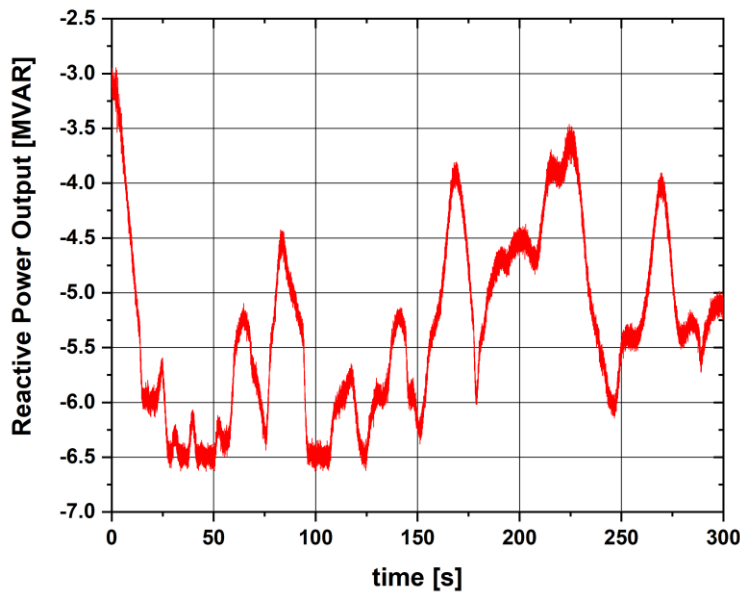


Figure 5.6: Reactive power output response in MVAR

Reactive power output both in MVAR and per unit has been presented in figures 5.6 and 5.7 respectively.

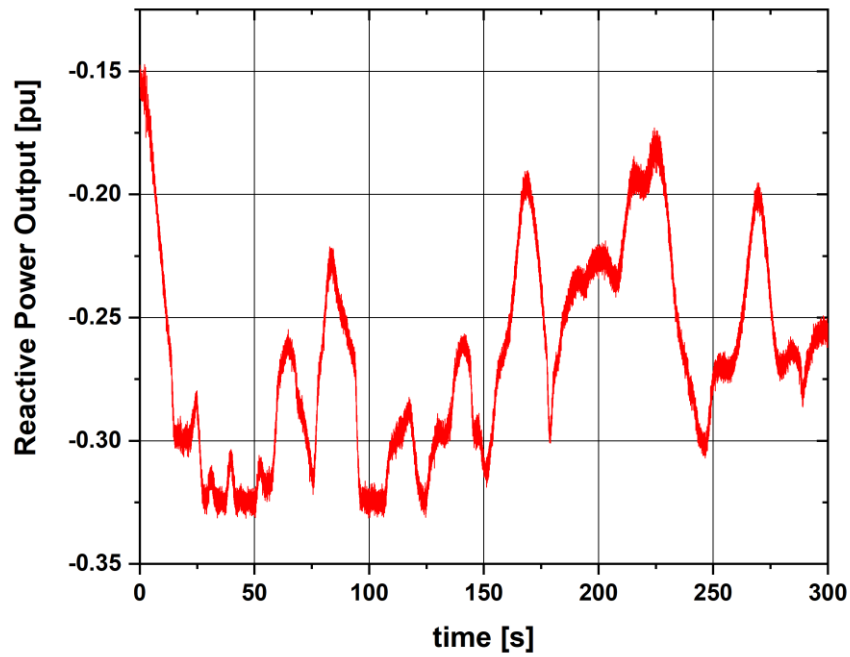


Figure 5.7: Reactive power output response in per unit

The terminal voltage as shown in figure 5.8 remains constant at 1.0 pu which confirms that the tuned PI controllers successfully augment the grid voltage fluctuation for the considered time.

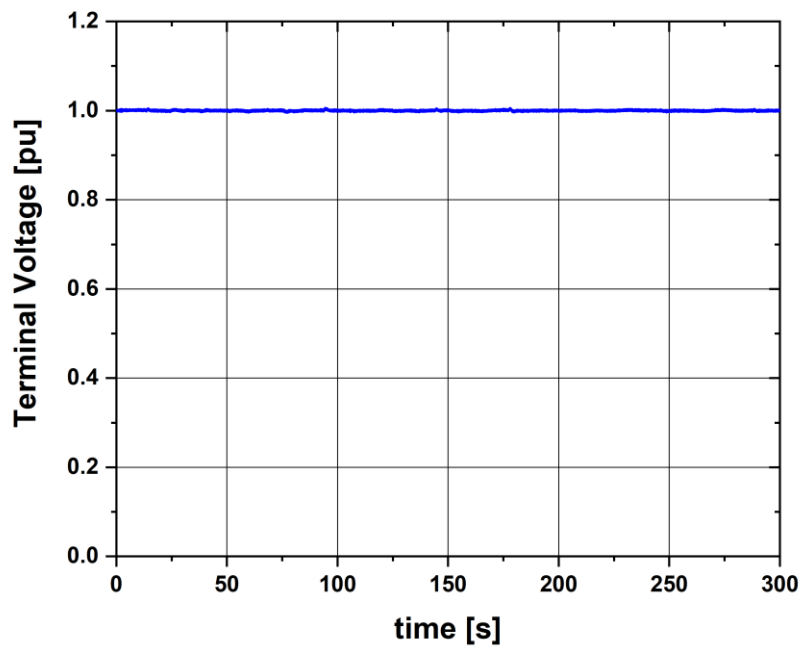


Figure 5.8: Terminal Voltage response

The frequency response characteristic of the power system is shown in figures 5.9 and 5.10. Figure 5.9 presents the zoomed scale of the frequency fluctuation which depicts that the variation lies under the permissible limit of the grid code ( $\pm 0.20$  Hz) as discussed in section 2.7. In this work, mainly the LVRT functionalities have been addressed, however, frequency fluctuations also lie under the permissible limit.

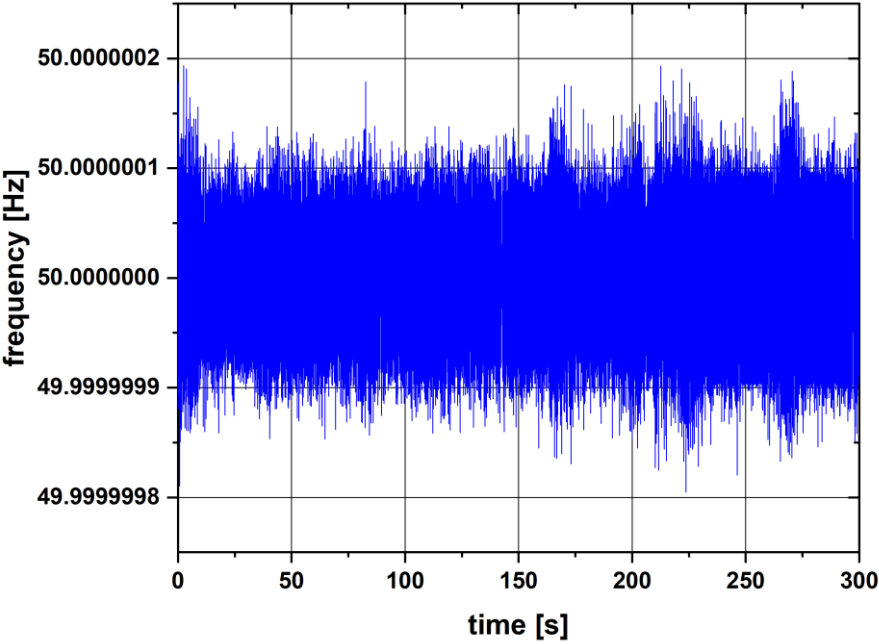


Figure 5.9: Frequency response characteristics of the power system (zoomed scale)

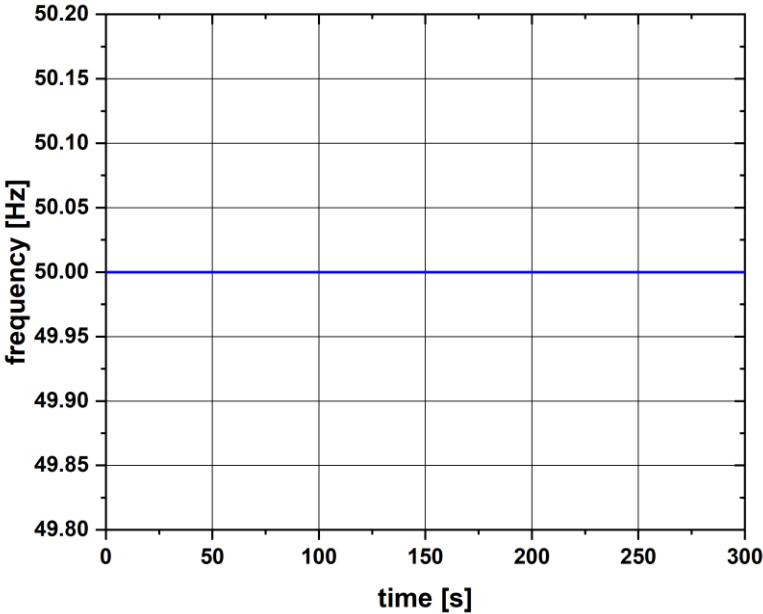


Figure 5.10: Frequency response characteristics of the power system

As depicted in figure 5.11, the DFIG's DC-link voltage remains almost constant. Although the wind speed varies greatly, the variation in the DC-link voltage is minimal as shown in figure 5.12.

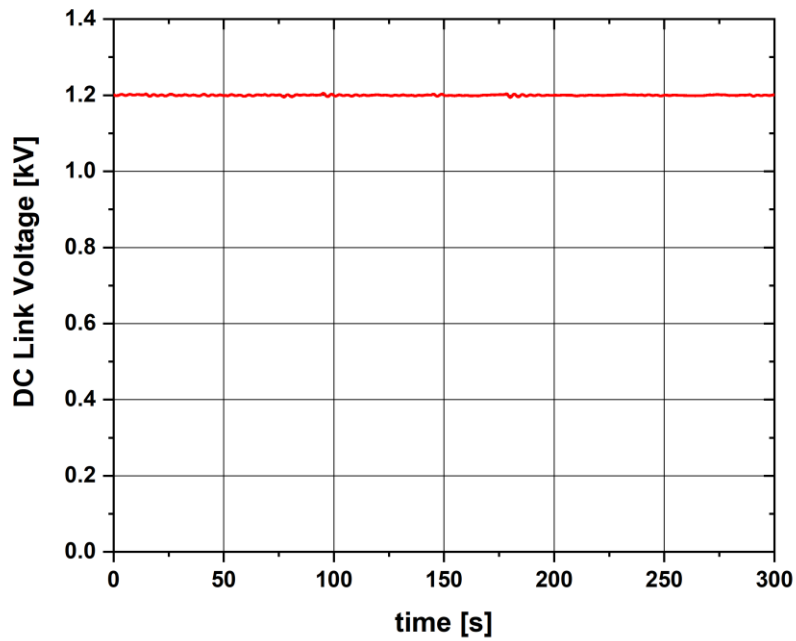


Figure 5.11: Response of DC Link voltage

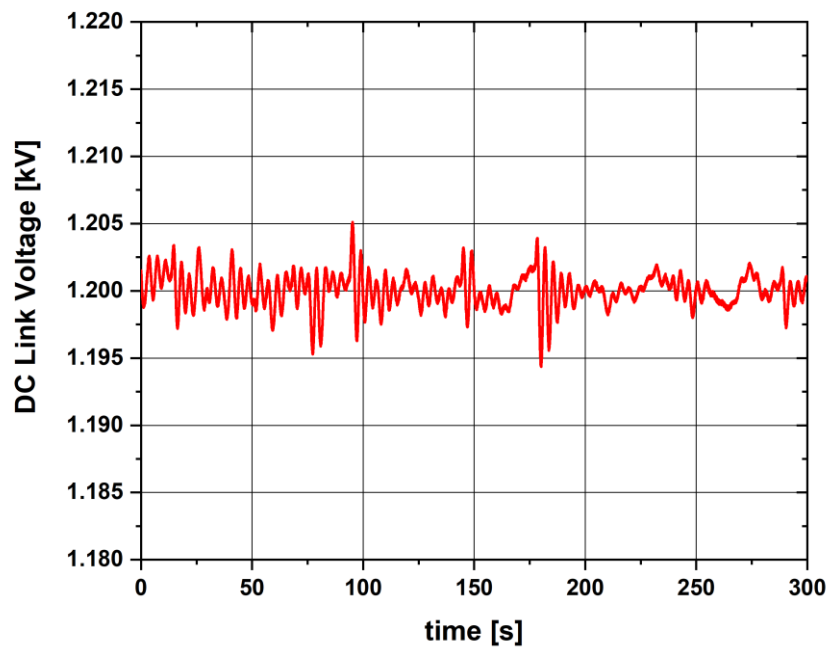


Figure 5.12: Response of DC Link voltage (zoomed scale)



Figure 5.13 presents the rotor speed response under varying wind speeds. According to the rotor speed response, it is seen that almost all the time the rotor is operating over speed mode ( $>1.0$  pu) due to the nature of DFIG's characteristics.

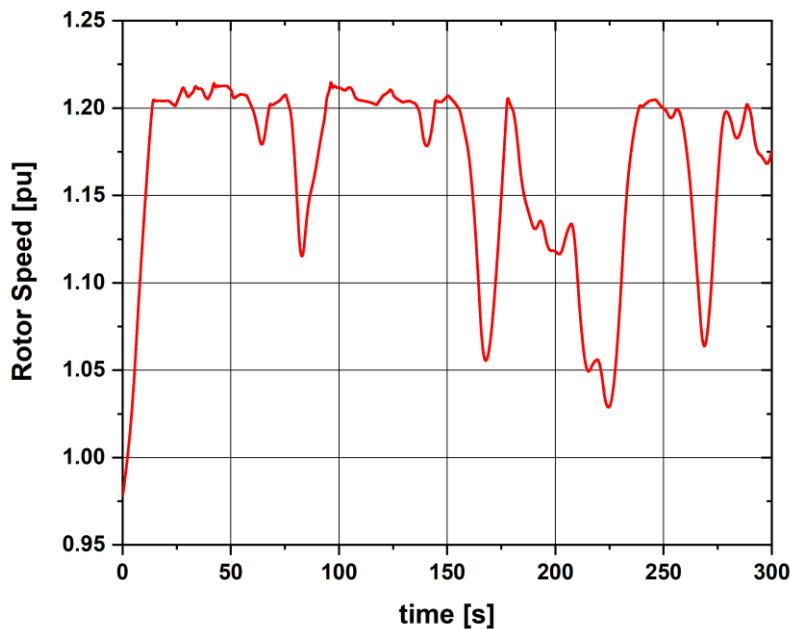


Figure 5.13: Rotor Speed response in per unit

### 5.3 Transient Stability Performance Analysis

Transient analysis is performed in a short period. In this work, the simulation runtime of the transient analysis is considered 10.0 seconds. The fault conditions are depicted in figure 5.14. Asymmetrical (1LG and 2LG) and most severe symmetrical 3LG faults have been considered in this work to analyse the performance of the model power system as well as the robustness of the tuned PI controllers.

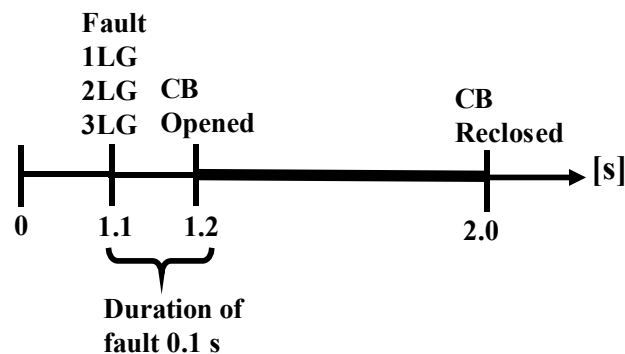


Figure 5.14: Fault condition for transient analysis

According to figure 5.14, fault has been applied on 1.1 sec at one of the transmission lines as shown in figure 5.1. The duration of the fault is 0.1 sec and 1.2 sec later, the two circuit breakers of the line are opened to isolate it from the power system. Circuit breakers are reclosed on 2.0 seconds considering the fault has been cleared. The wind speed of the turbine has been kept at the rated value as shown in figure 5.15 which is 12.5 m/s. This is because wind speed does not fluctuate significantly in the short span of time (10 sec).

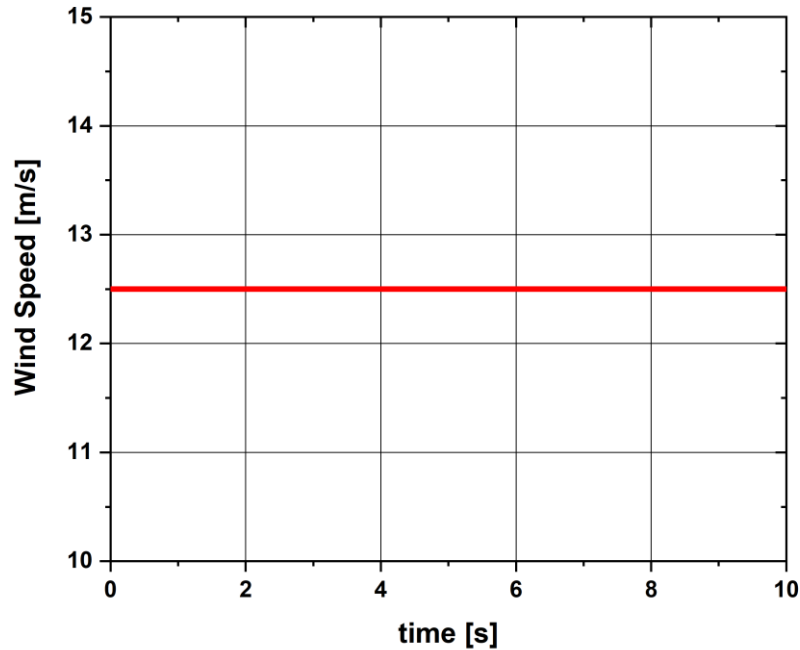


Figure 5.15: Wind speed at the rated condition for transient analysis

As depicted in figure 5.16, due to faults applied on 1.1 second, terminal voltage drops significantly below the 1.0 pu. The voltage dip is more significant in the case of the most severe symmetrical 3LG fault. In order to comply with the modern grid code standards as discussed in section 2.5, 90 percent of the voltage must be restored to pre-fault levels in 1500 milliseconds or 1.5 seconds after the fault. In our case, the terminal voltage has recovered to 90 percent of its pre-fault value within 500 milliseconds or 0.5 seconds after the fault. It is also evident that the terminal voltage has attained exactly 1.0 pu at steady state for all types of faults. However, some overshoot has been observed, which is negligible and obvious for such type of fault condition. Thus, it can be said that the tuned PI controllers successfully augment the voltage stability of the designed model power system.

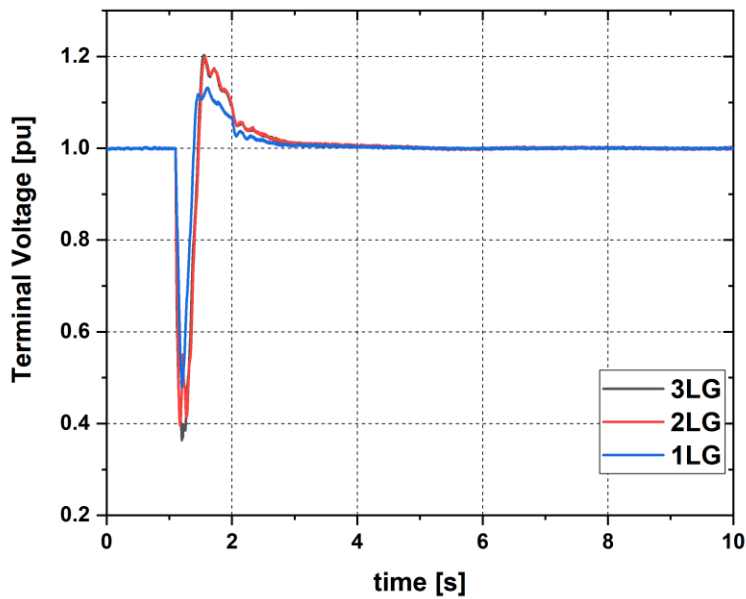


Figure 5.16: Terminal Voltage under different types of faults

Figure 5.17 and 5.18 depict active power output response in MW and per unit respectively under different types of faults. It has been observed that 2LG and 3LG faults have the most severe impact during the fault period. However, around 4 seconds active output power started to reach around the rated generator's capacity which is 20 MW or 1.0 pu. Some overshoot has been observed in the case of the 2LG and 3LG fault scenario but in the normal or steady-state, active output power response reaches the stable state.

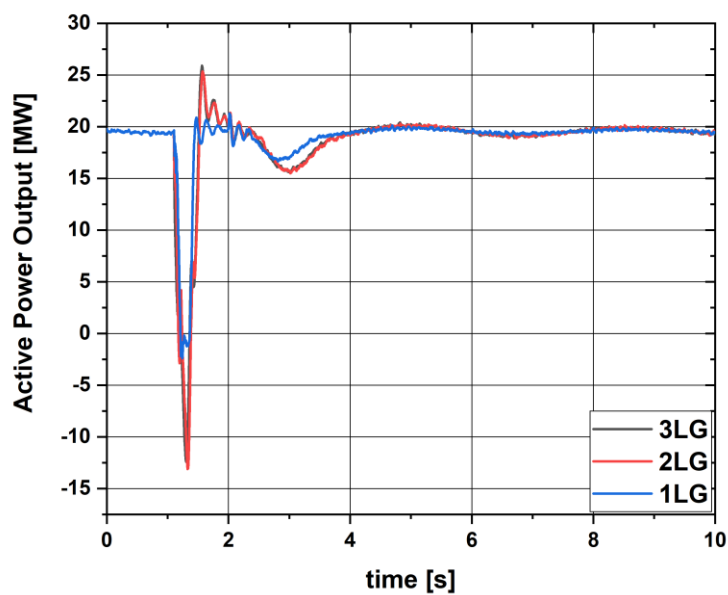


Figure 5.17: Active power output response in MW under different types of faults

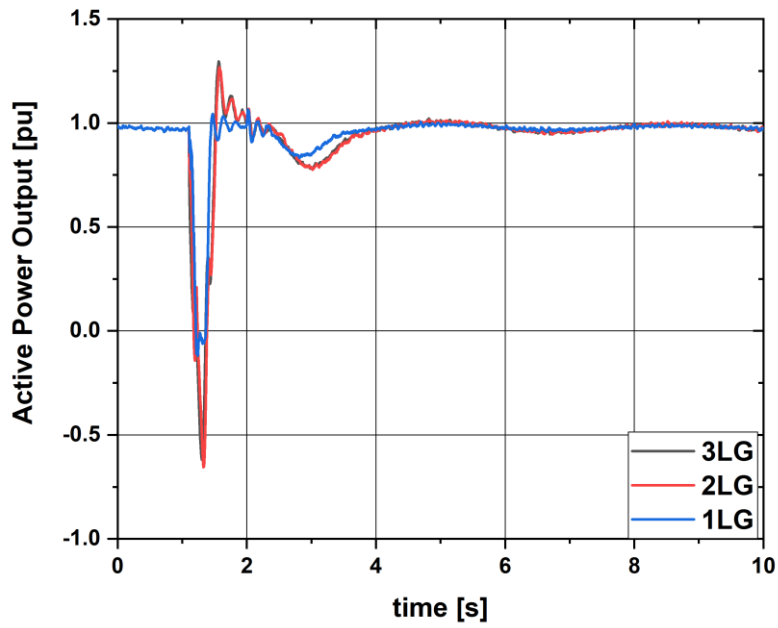


Figure 5.18: Active power output response in per unit under different types of faults

The reactive power output response in MVAR and per unit has been presented in figures 5.19 and 5.20 respectively. During the fault phase, reactive power injection from the generator to the grid is maximum in the case of 2LG and 3LG fault scenarios which are 14 MVAR or 0.99 pu for both cases. For the fault case of 1LG, it is around 5 MVAR or 0.25 pu. Reactive power injection is important to keep the terminal voltage at 1.0 pu

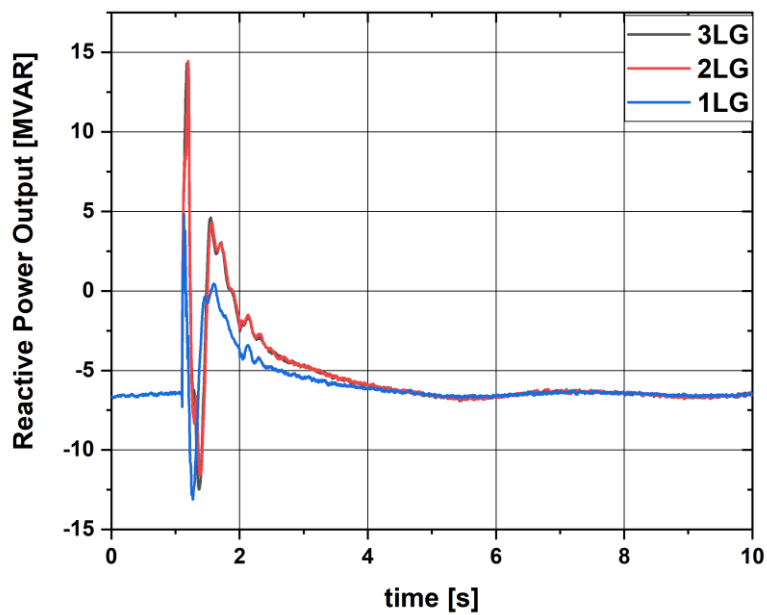


Figure 5.19: Reactive power output response in MVAR under different types of faults

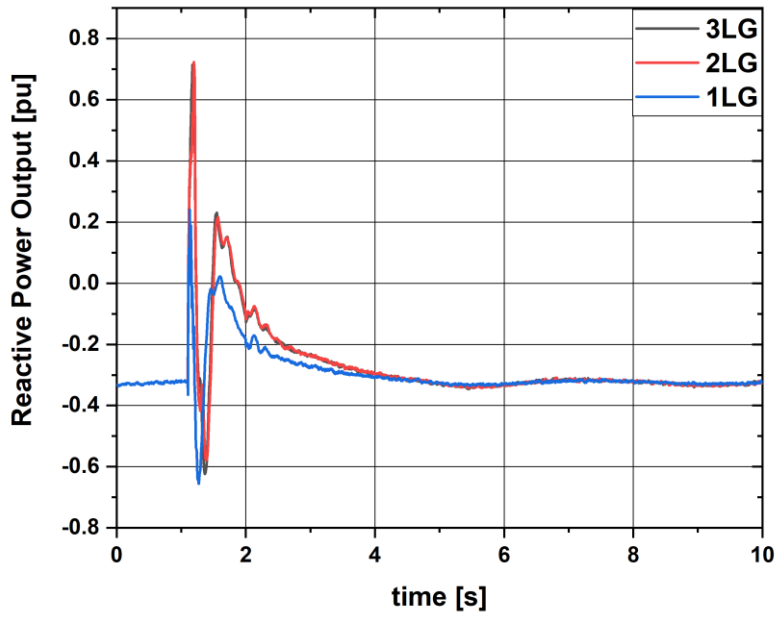


Figure 5.20: Reactive power output response in per unit under different types of faults

The frequency response characteristics of the power system is shown in figures 5.21 and 5.22. Figure 5.21 presents the zoomed scale of the frequency fluctuation which depicts that the variation lies under the permissible limit of the grid code ( $\pm 0.20$  Hz) as discussed in section 2.7. In this work, mainly the LVRT functionalities have been addressed, however, frequency fluctuations also lie under the permissible limit.

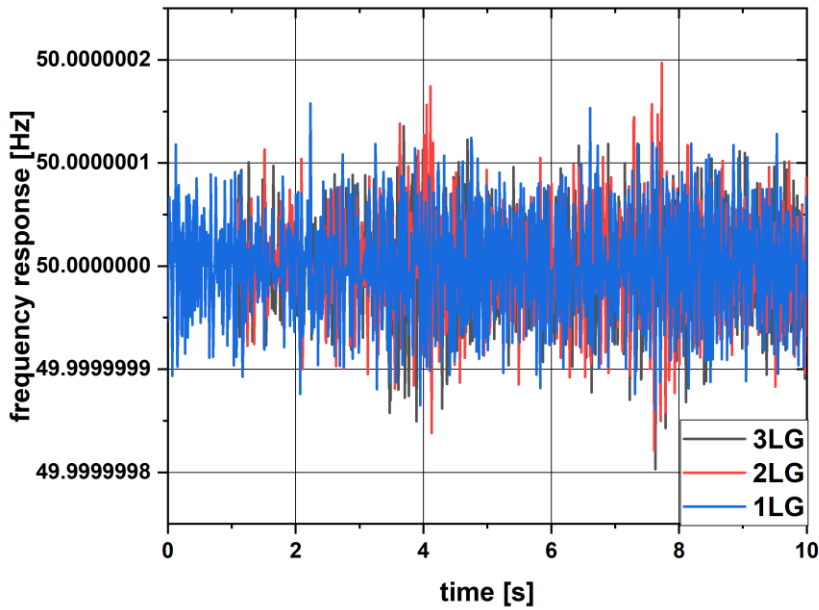


Figure 5.21: Frequency response characteristics under various types of faults (zoomed scale)

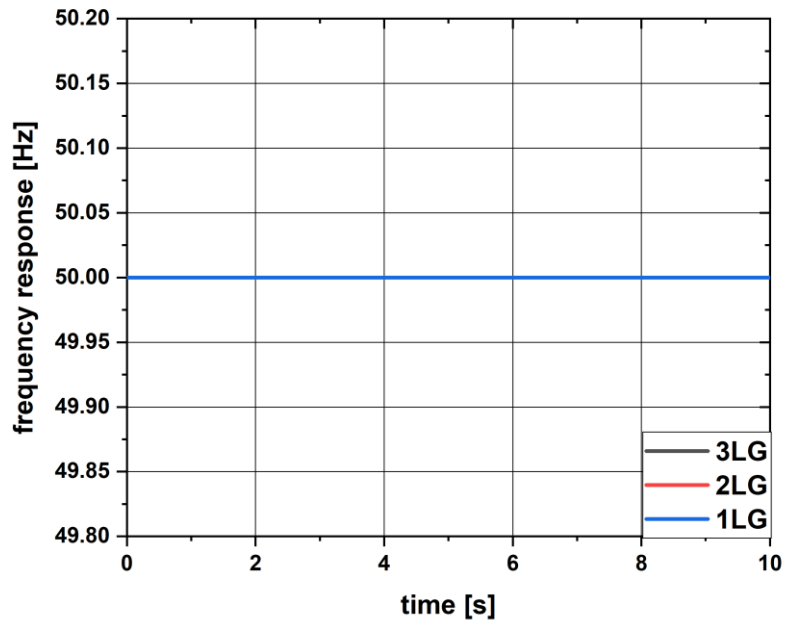


Figure 5.22: Frequency response characteristics under different types of faults

DC link voltage response under different fault scenarios has been presented in figure 5.23. For different fault conditions, DC link voltage stays near to the rated value which is 1.2 kV.

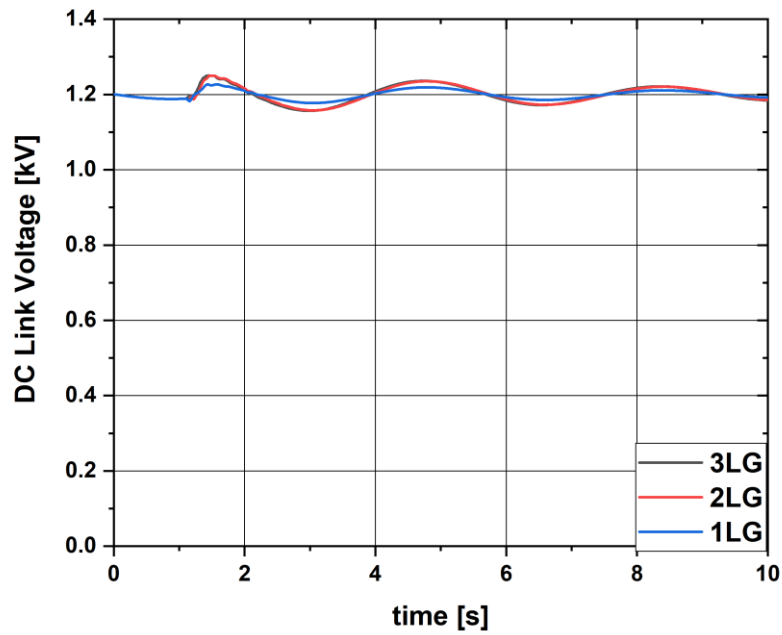


Figure 5.23: DC link voltage under different types of faults

Rotor speed under different fault scenarios has been presented in figure 5.24. Rotor speed rises to maximum during fault period, but it reaches near to rated speed condition very quickly after the fault period.

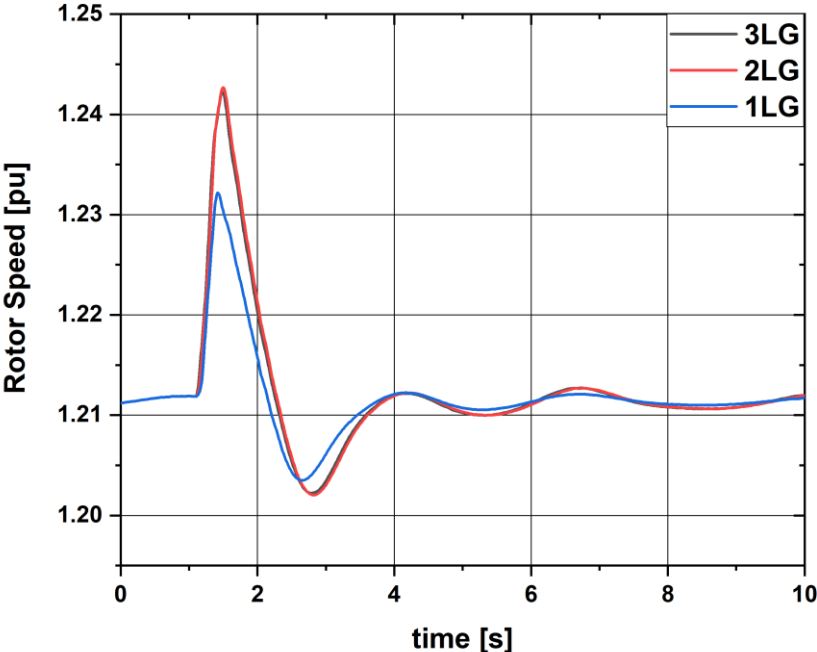


Figure 5.24: Rotor speed in per unit under different types of faults

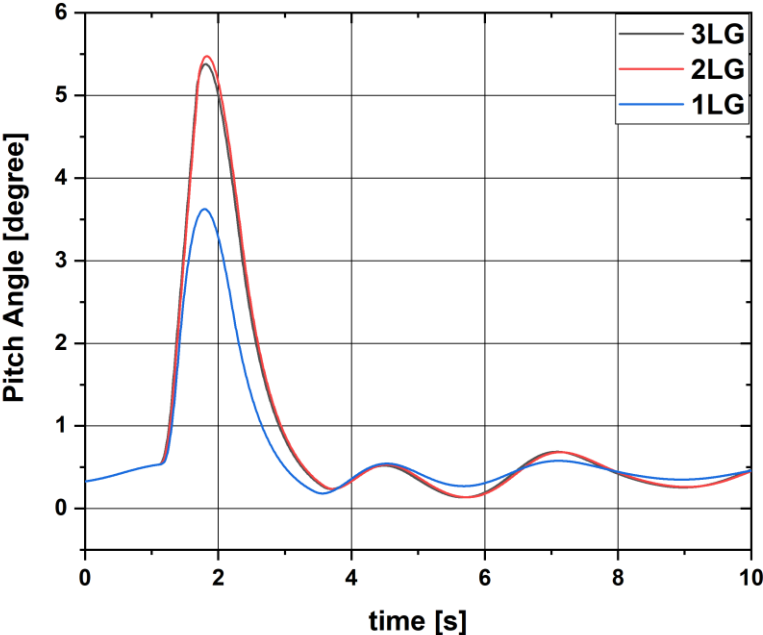


Figure 5.25: Pitch angle response under different types of faults

Figure 5.25 presents the pitch angle response under different types of fault scenarios. The pitch controller should work only when the wind speed is greater than the rated speed which is 12.5 m/s. Although it is observed that during the fault period the pitch angle controller comes into operation due to a sudden drop in voltage level and increased rotor speed. As shown in figures 5.24 and 5.25, the pitch controller is dependent on the rotor speed variation. Whenever rotor speed increases from the rated speed of 1.21 pu, the pitch controller comes into operation to stabilize the turbine blade. During fault period, a surge in rotor speed has been observed due to the maximum injection of reactive power from generator to grid with a view to stabilizing the terminal voltage.

## 5.4 Chapter Summary

This chapter provides graphical representation of various analyses that have been observed during the PSCAD/EMTDC simulation. A complete power system model that is linked to an infinite bus has been considered to observe the resilience of the system. Analyses have been carried both for the dynamic and transient conditions. Transient analysis has been performed for a short period of 10 seconds assuming wind speed does not fluctuate significantly during this short period whereas dynamic simulation has been performed for longer period of 300 seconds. Fault analysis considering the most severe 3LG fault has been examined with a view to assessing the voltage stability and LVRT criterion of the grid code. Simulation results show that tuned PI controllers effectively augment the LVRT functionality by injecting maximum reactive power of 14 MVAR and 5 MVAR into the grid during 3LG/2LG and 1LG faults respectively. It is also observed that the terminal voltage has recovered to 90 percent of its pre-fault level within 500 milliseconds or 0.5 seconds after the fault. Moreover, the DFIG's active power output response stays at the rated capacity during steady-state for both transient and dynamic conditions. It is also evident that the terminal voltage has attained exactly 1.0 pu at steady state for all types of faults.





## 6 Conclusion and Future Work

The goal of this thesis is to demonstrate LVRT augmentation of a grid-tied DFIG-based wind turbine. Voltage stability is one of the critical grid code requirements which needs to be maintained strictly. During fault or network disturbance situation, significant voltage dip occurs which needs to be recovered as fast as possible. Modern grid code implies that the 90% of the voltage needs to be recovered to pre-fault value within 1500 milliseconds or 1.5 seconds. Thus, it is essential to perform both dynamic and transient analyses to assess the LVRT capabilities of the designed power system. Dynamic analysis has been performed for longer durations (300 seconds) under real wind speed data of Hokkaido island in Japan, on the other hand, transient analysis has been performed under fixed wind speed condition considering wind speed does not fluctuate for a short period of 10 seconds. Fault analysis including the most severe 3LG fault has been considered in transient conditions with a view to assessing the tuned PI controller scheme and robustness of the designed power system model. PSCAD/EMTDC simulation tool has been used extensively to design the DFIG wind turbine aerodynamic model, DFIG control scheme and power system model analysis. PI controllers of the RSC and GSC have been tuned experimentally. In order to achieve optimized values of PI controllers, several simulations have been conducted under different values of PI gain constants.

It has been observed that tuned PI controllers successfully augment the LVRT functionalities by injecting adequate reactive power to the grid during fault or network disturbance situations. Under transient analysis, the terminal voltage has recovered to 90% of its pre-fault value within 500 milliseconds or 0.5 seconds after the fault. It is also evident that the terminal voltage has attained exactly 1.0 pu at steady state for all types of faults. During the transient fault period, reactive power injection from the generator to the grid is maximum in the case of 2LG and 3LG fault scenarios which are 14 MVAR or 0.99 pu for both cases. For the transient fault case of 1LG, it is around 5 MVAR or 0.25 pu. Moreover, the DFIG's active power output response stays at the rated capacity (20 MW) during steady-state for both transient and dynamic conditions.

Some notable key suggestions for broadening the scope of this work are summarized as follows:

- I. In this work, the used PI controllers have fixed parameter gain constants that are not adaptive based on the system change for the large-scale power system. Also, the tuning of the PI controllers is cumbersome and time inefficient. Thus, in the case of large power systems, the conventional PI controllers fail to inject enough reactive power during the fault or network disturbance situations. So, it is recommended to use more advanced control strategies like fuzzy-PI, artificial neural networks, or other adaptive control schemes to augment the LVRT capabilities of the large-scale power system. Although the LVRT competency can be enhanced, the computational obligation for employing these intelligent controllers is very high. Furthermore, the success of employing such an intelligent control algorithm mainly depends upon the experience of the designer. Other hardware-based auxiliary control strategies like FACTS devices are also an option but cost is always an important concern in this regard.
- II. Voltage, as well as frequency stability, are the two most important grid code requirements which need to be maintained strictly. In this work, only voltage stability control has been addressed. So, it is also important to work on the frequency stability issues by employing control schemes like droop controller, virtual inertia controller, etc.
- III. Varying wind speed turbine like DFIG is costly due to the partially rated semiconductor converter. On the other hand, a fixed-speed wind turbine like SCIG is simpler and less costly than DFIG. But the capacitor bank of the SCIG can not provide enough reactive power during fault or network disturbance situations which failed the LVRT capabilities of the grid. So, an ideal option could be the hybridization of wind farms by installing a low-capacity DFIG wind turbine with a higher capacity SCIG wind turbine. Thus, cost optimization, as well as LVRT augmentation could be served.
- IV. In this thesis work, an infinite bus has been considered in the power system model. An infinite bus has active and reactive power capabilities with fixed frequency

and voltage ratings. So, for more realistic simulation, IEEE 9 bus or IEEE 13 bus systems could be ideal options in future works.

- V. In future work, it is also crucial to do research on the features of the wind speed restriction and the control mechanism to handle the situation when the wind speed falls or fluctuates lower than the speed at the rated condition.



# Bibliography

- [1] 'Global Energy Review 2021', p. 36, 2021.
- [2] John Andrews, Nicholas Alfred Jelley, and Nick Jelley, *Energy Science: Principles, Technologies, and Impacts*. OUP Oxford, 2007.
- [3] 'FUTURE OF WIND: Deployment, investment, technology, grid integration and socio-economic aspects (A Global Energy Transformation paper)', International Renewable Energy Agency (IRENA), Abu Dhabi, Oct. 2019.
- [4] '2022 renewable energy industry outlook', Deloitte, 2022.
- [5] 'Renewable energy sources and climate change mitigation: special report of the Intergovernmental Panel on Climate Change', *Choice Rev. Online*, vol. 49, no. 11, pp. 49-6309-49-6309, Jul. 2012, doi: 10.5860/CHOICE.49-6309.
- [6] 'Renewables 2021 - Analysis and forecast to 2026', p. 175, 2021.
- [7] 'Renewable Energy Statistics 2021', p. 460.
- [8] International Energy Agency, *Renewable Energy Market Update: Outlook for 2020 and 2021*. OECD, 2020. doi: 10.1787/afbc8c1d-en.
- [9] 'Renewables 2020 - Analysis and forecast to 2025', p. 172, 2020.
- [10] 'RENEWABLES 2021 GLOBAL STATUS REPORT (GSR 2021)', REN21, 2021.
- [11] J. C. Smith, A. D. Broe, A. Estanquero, and G. Duclos, 'WIND ENERGY - THE FACTS - GRID INTEGRATION', p. 44, 2009.
- [12] J. Valinejad *et al.*, 'Long-Term Decision on Wind Investment with Considering Different Load Ranges of Power Plant for Sustainable Electricity Energy Market', *Sustainability*, vol. 10, no. 10, p. 3811, Oct. 2018, doi: 10.3390/su10103811.
- [13] J. Valinejad, T. Barforoshi, M. Marzband, E. Pouresmaeil, R. Godina, and J. P. S. Catalão, 'Investment Incentives in Competitive Electricity Markets', *Appl. Sci.*, vol. 8, no. 10, p. 1978, Oct. 2018, doi: 10.3390/app8101978.
- [14] M. Javadi, M. Marzband, M. Funsho Akorede, R. Godina, A. Saad Al-Sumaiti, and E. Pouresmaeil, 'A Centralized Smart Decision-Making Hierarchical Interactive Architecture for Multiple Home Microgrids in Retail Electricity Market', *Energies*, vol. 11, no. 11, p. 3144, Nov. 2018, doi: 10.3390/en11113144.
- [15] P. Jain and P. Wijayatunga, 'Grid Integration of Wind Power: Best Practices for Emerging Wind Markets', p. 36.
- [16] Joyce Lee and Feng Zhao, 'Global Wind Report 2021', Global Wind Energy Council (GWEC), 2021.
- [17] T. Ackermann, Ed., *Wind power in power systems*, 2nd ed. Chichester, West Sussex ; Hoboken, N.J: Wiley, 2012.
- [18] P. Kundur, *Power System Stability and Control*. McGraw Hill, 1994.
- [19] J. W. Simpson-Porco, F. Dörfler, and F. Bullo, 'Voltage collapse in complex power grids', *Nat. Commun.*, vol. 7, no. 1, p. 10790, Apr. 2016, doi: 10.1038/ncomms10790.
- [20] F. A. Shaikh, M. S. Alam, M. S. J. Asghar, and F. Ahmad, 'Blackout Mitigation of Voltage Stability Constrained Transmission Corridors through Controlled Series Resistors', *Recent Adv. Electr. Electron. Eng. Former. Recent Pat. Electr. Electron. Eng.*, vol. 11, no. 1, Jan. 2018, doi: 10.2174/2352096510666171108160930.
- [21] Y. Li, 'Analysis of 1996 Western American Electric Blackouts', p. 37.

- [22] H. Haes Alhelou, M. Hamedani-Golshan, T. Njenda, and P. Siano, 'A Survey on Power System Blackout and Cascading Events: Research Motivations and Challenges', *Energies*, vol. 12, no. 4, p. 682, Feb. 2019, doi: 10.3390/en12040682.
- [23] Md. Hazari, M. Mannan, S. Muyeen, A. Umemura, R. Takahashi, and J. Tamura, 'Stability Augmentation of a Grid-Connected Wind Farm by Fuzzy-Logic-Controlled DFIG-Based Wind Turbines', *Appl. Sci.*, vol. 8, no. 1, p. 20, Dec. 2017, doi: 10.3390/app8010020.
- [24] A. Moghadasi, A. Sarwat, and J. M. Guerrero, 'A comprehensive review of low-voltage-ride-through methods for fixed-speed wind power generators', *Renew. Sustain. Energy Rev.*, vol. 55, pp. 823–839, Mar. 2016, doi: 10.1016/j.rser.2015.11.020.
- [25] Y. Chi, Y. Liu, W. Wang, and H. Dai, 'Voltage Stability Analysis of Wind Farm Integration into Transmission Network', in *2006 International Conference on Power System Technology*, Chongqing, China, Oct. 2006, pp. 1–7. doi: 10.1109/ICPST.2006.321661.
- [26] S. Mali, S. James, and I. Tank, 'Improving Low Voltage Ride-through Capabilities for Grid Connected Wind Turbine Generator', *Energy Procedia*, vol. 54, pp. 530–540, 2014, doi: 10.1016/j.egypro.2014.07.294.
- [27] M. Martins, 'Voltage Stability Issues Related to Implementation of Large Wind Farms', p. 66.
- [28] M. Alam, M. Abido, A. Hussein, and I. El-Amin, 'Fault Ride through Capability Augmentation of a DFIG-Based Wind Integrated VSC-HVDC System with Non-Superconducting Fault Current Limiter', *Sustainability*, vol. 11, no. 5, p. 1232, Feb. 2019, doi: 10.3390/su11051232.
- [29] K. E. Okedu, 'Stabilization of Grid Connected Wind Farm by DFIG-based Variable Speed Wind Turbine', Doctor of Engineering Thesis, Kitami Institute of Technology, Japan, Japan, 2012.
- [30] K. Okedu, *Enhanced Power Grid Stability Using Doubly-Fed Induction Generators*. AIP Publishing, 2020. doi: 10.1063/9780735422292.
- [31] 'E. ON NETZ GmbH, Grid Connection Regulation for High and Extra High Voltage', Essen, Germany, 2006.
- [32] Md. R. Hazari *et al.*, 'Stabilization Control of Power System with Large-Scale Wind Farm by Using DFIG Considering Grid Codes', in *2019 International Conference on Robotics, Electrical and Signal Processing Techniques (ICREST)*, Dhaka, Bangladesh, Jan. 2019, pp. 102–107. doi: 10.1109/ICREST.2019.8644524.
- [33] M. F. El-Naggar, M. I. Mosaad, H. M. Hasanien, T. A. AbdulFattah, and A. F. Bendary, 'Elephant herding algorithm-based optimal PI controller for LVRT enhancement of wind energy conversion systems', *Ain Shams Eng. J.*, vol. 12, no. 1, pp. 599–608, Mar. 2021, doi: 10.1016/j.asej.2020.07.013.
- [34] O. S. Elazab, M. Debouza, H. M. Hasanien, S. M. Muyeen, and A. Al-Durra, 'Salp swarm algorithm-based optimal control scheme for LVRT capability improvement of grid-connected photovoltaic power plants: design and experimental validation', *IET Renew. Power Gener.*, vol. 14, no. 4, pp. 591–599, Mar. 2020, doi: 10.1049/iet-rpg.2019.0726.
- [35] Md. R. Hazari, E. Jahan, M. A. Mannan, and J. Tamura, 'Coordinated Control Scheme of Battery Storage System to Augment LVRT Capability of SCIG-Based Wind Turbines and Frequency Regulation of Hybrid Power System', *Electronics*, vol. 9, no. 2, p. 239, Feb. 2020, doi: 10.3390/electronics9020239.
- [36] H. Y. Mahmoud, H. M. Hasanien, A. H. Besheer, and A. Y. Abdelaziz, 'Hybrid cuckoo search algorithm and grey wolf optimiser-based optimal control strategy for performance enhancement of HVDC-based offshore wind farms', *IET Gener.*

- Transm. Distrib.*, vol. 14, no. 10, pp. 1902–1911, May 2020, doi: 10.1049/iet-gtd.2019.0801.
- [37] N. Hosseinzadeh, A. Aziz, A. Mahmud, A. Gargoom, and M. Rabbani, ‘Voltage Stability of Power Systems with Renewable-Energy Inverter-Based Generators: A Review’, *Electronics*, vol. 10, no. 2, p. 115, Jan. 2021, doi: 10.3390/electronics10020115.
- [38] H. M. Hasanien and S. M. Muyeen, ‘A Taguchi Approach for Optimum Design of Proportional-Integral Controllers in Cascaded Control Scheme’, *IEEE Trans. Power Syst.*, vol. 28, no. 2, pp. 1636–1644, May 2013, doi: 10.1109/TPWRS.2012.2224385.
- [39] K. Z. Heetun, S. H. E. Abdel Aleem, and A. F. Zobaa, ‘Voltage stability analysis of grid-connected wind farms with FACTS: Static and dynamic analysis’, *Energy Policy Res.*, vol. 3, no. 1, pp. 1–12, Jan. 2016, doi: 10.1080/23317000.2015.1128369.
- [40] X. Luo *et al.*, ‘Review of Voltage and Frequency Grid Code Specifications for Electrical Energy Storage Applications’, *Energies*, vol. 11, no. 5, p. 1070, Apr. 2018, doi: 10.3390/en11051070.
- [41] A. Annamraju and S. Nandiraju, ‘Coordinated control of conventional power sources and PHEVs using jaya algorithm optimized PID controller for frequency control of a renewable penetrated power system’, *Prot. Control Mod. Power Syst.*, vol. 4, no. 1, p. 28, Dec. 2019, doi: 10.1186/s41601-019-0144-2.
- [42] J. M. Akanto, Md. R. Hazari, and M. A. Mannan, ‘LVRT and Stability Enhancement of Grid-Tied Wind Farm Using DFIG-Based Wind Turbine’, *Appl. Syst. Innov.*, vol. 4, no. 2, p. 33, May 2021, doi: 10.3390/asi4020033.
- [43] D. Chatterjee, *Modelling and Control of DFIG-based Variable Speed Wind Turbine*.
- [44] M. Singh and S. Santoso, ‘Dynamic Models for Wind Turbines and Wind Power Plants’, NREL/SR-5500-52780, 1028524, Oct. 2011. doi: 10.2172/1028524.
- [45] M. Zribi, M. Alrifai, and M. Rayan, ‘Sliding Mode Control of a Variable-Speed Wind Energy Conversion System Using a Squirrel Cage Induction Generator’, *Energies*, vol. 10, no. 5, p. 604, May 2017, doi: 10.3390/en10050604.
- [46] M. Rosyadi, A. Umemura, R. Takahashi, J. Tamura, N. Uchiyama, and K. Ide, ‘Simplified Model of Variable Speed Wind Turbine Generator for Dynamic Simulation Analysis’, *IEEJ Trans. Power Energy*, vol. 135, no. 9, pp. 538–549, 2015, doi: 10.1541/ieejpes.135.538.
- [47] M. Gustavo and P. Enrique, ‘Modelling and Control Design of Pitch-Controlled Variable Speed Wind Turbines’, in *Wind Turbines*, I. H. Al-Bahadly, Ed. InTech, 2011. doi: 10.5772/15880.
- [48] M. Gustavo and J. Gimenez, ‘Technical and Regulatory Exigencies for Grid Connection of Wind Generation’, in *Wind Farm - Technical Regulations, Potential Estimation and Siting Assessment*, G. O. Suvire, Ed. InTech, 2011. doi: 10.5772/16474.
- [49] B. Fox, Ed., *Wind power integration: connection and system operational aspects*. London: Institution of Engineering and Technology, 2007.
- [50] Raymond W. Flumerfelt, and Su Su Wang, *Wind Turbines*. ©McGraw-Hill Companies, 2009. [Online]. Available: <http://www.accessscience.com>
- [51] X. Yang, G. Liu, A. Li, and L. V. Dai, ‘A Predictive Power Control Strategy for DFIGs Based on a Wind Energy Converter System’, *Energies*, vol. 10, no. 8, p. 1098, Jul. 2017, doi: 10.3390/en10081098.
- [52] B. Pokharel, ‘MODELING, CONTROL AND ANALYSIS OF A DOUBLY FED INDUCTION GENERATOR BASED WIND TURBINE SYSTEM WITH VOLTAGE REGULATION’, p. 336.
- [53] ‘Wind power in Brazil and the US’. <https://sites.google.com/site/comparingwindpower/> (accessed Feb. 18, 2022).



- [54] H. Meng, T. Yang, J. Liu, and Z. Lin, 'A Flexible Maximum Power Point Tracking Control Strategy Considering Both Conversion Efficiency and Power Fluctuation for Large-inertia Wind Turbines', *Energies*, vol. 10, no. 7, p. 939, Jul. 2017, doi: 10.3390/en10070939.
- [55] Md. Rifat Hazari, M. Abdul Mannan, S. M. Muyeen, A. Umemura, R. Takahashi, and J. Tamura, 'Fuzzy Logic based Virtual Inertia Control of DFIG based Wind Generator for Stability Improvement of Hybrid Power System', *IEEJ Trans. Power Energy*, vol. 138, no. 8, pp. 733–744, Aug. 2018, doi: 10.1541/ieejpes.138.733.
- [56] L. Sartika, 'Operation and Control of VSC based Grid Connected Wind Farm', p. 104.
- [57] M. ROSYADI, 'Stability Augmentation of Grid Connected Wind Farm by Variable Speed Permanent Magnet Wind Generator', Kitami Institute of Technology, Japan, 2013.
- [58] 'PSCAD User's Guide'. <https://www.pscad.com/knowledge-base/article/160> (accessed Mar. 13, 2022).
- [59] Md. R. Hazari, 'Stability Enhancement of Grid-Connected Wind Farm and Hybrid Power System by Variable Speed Wind Generators', Doctoral Thesis, Kitami Institute of Technology, Japan, 2019.
- [60] Lee, Dong-Choon, 'Developing Function Models of Back-to-Back PWM Converters for Simplified Simulation', *J. Power Electron.*, vol. 11, no. 1, pp. 51–58, Jan. 2011, doi: 10.6113/JPE.2011.11.1.051.
- [61] N. S. Nise, *Control System Engineering*, 8th ed. Wiley, 2019.
- [62] 'Hokkaido island wind speed data'. <https://github.com/msajidh/sajid/blob/main/Hokkaido%20island%20wind%20speed%20data.xlsx> (accessed Jun. 13, 2022).